

# Dimer piling problems and interacting field theory

Rolando Ramirez Camasca and John McGreevy

*Department of Physics, University of California San Diego, La Jolla, CA 92093,  
USA*

## Abstract

The dimer tiling problem asks in how many ways can the edges of a graph be covered by dimers so that each site is covered once. In the special case of a planar graph, this problem has a solution in terms of a free fermionic field theory. We rediscover and explore an expression for the number of coverings of an arbitrary graph by arbitrary objects in terms of an interacting fermionic field theory first proposed by Samuel. Generalizations of the dimer tiling problem, which we call ‘dimer piling problems,’ demand that each site be covered  $N$  times by indistinguishable dimers. Our field theory provides a solution of these problems in the large- $N$  limit. We give a similar path integral representation for certain lattice coloring problems.

2023/12/22

# Contents

|          |   |           |
|----------|---|-----------|
| <b>1</b> | <b>Introduction</b>   | <b>3</b>  |
| <b>2</b> | <b>Integral representation of the general dimer problem</b> | <b>4</b>  |
| <b>3</b> | <b>Dimer piling problems</b>                                | <b>7</b>  |
| 3.1      | Feynman rules . . . . .                                     | 9         |
| 3.2      | Combinatorial problems from grassmann integrals . . . . .   | 9         |
| <b>4</b> | <b>Large-<math>N</math> analysis</b>                        | <b>13</b> |
| 4.1      | Saddle point analysis . . . . .                             | 16        |
| 4.2      | Large- $N$ Feynman diagrams . . . . .                       | 24        |
| <b>5</b> | <b>Graph coloring problems</b>                              | <b>29</b> |
| <b>6</b> | <b>Discussion</b>   | <b>32</b> |
| <b>A</b> | <b>Combinatorial problems on dimer pilings</b>              | <b>37</b> |
| <b>B</b> | <b>Transfer matrix</b>                                      | <b>41</b> |
| <b>C</b> | <b>Details of saddle point calculation</b>                  | <b>45</b> |
|          | <b>References</b>   | <b>50</b> |

# 1 Introduction

The dimer tiling problem for a graph  $\Gamma$  asks in how many ways can we place dimers on the edges of  $\Gamma$  such that every vertex is covered by a single dimer. In the special case of a *planar* graph, this (fully-packed) dimer tiling problem is exactly solvable [1, 2, 3, 4, 5, 6, 7]. One representation of the solution is as an integral over grassmann variables at the sites of the graph, with a gaussian measure determined by a signed adjacency matrix of the graph. The signs are chosen so that there is  $\pi$  flux through each plaquette of the graph, and this weights each dimer configuration with a + sign. Such a weighting is not possible on a non-planar graph.

The dimer tiling problem admits many generalizations. For example, we could allow monomers, or sites that are not covered by dimers. More generally, one can introduce the following partition function describing coverings by monomers and dimers even on non-planar graphs:

$$Z(\Gamma, x) = \sum_{\text{dimer configurations on } \Gamma} x^{\#\text{of monomers}} \quad (1.1)$$

where the sum runs over dimer configurations that cover each site of  $\Gamma$  at most once; uncovered sites are called monomers and are weighted with monomer fugacity  $x$ . Even on a planar graph, the monomer-dimer problem is not exactly solvable.

Many other generalizations of the dimer problem have been studied. We could weight the dimers of different orientation differently. We could replace the dimers by objects of a different shape, such as linear trimers [8, 9] or wedges, or sphinxes [10].

A family of generalizations on which we will focus is where the number of dimers incident on each site is  $N$  instead of just 1. We call such generalizations *dimer piling problems*. Our main contribution is an integral representation for three large- $N$  generalizations (for certain weights of the configurations) that turns out to be solvable by standard field theory methods.

The  $N = 1$  version of this integral representation was studied previously in [11, 12, 13]. Even at finite  $N$ , it can be used as a starting point for an auxiliary-field Monte Carlo evaluation of these partition functions.

Other graph coloring problems can be also studied along the same lines. In particular, we show that the problem of counting  $N$ -colorings of the links of a graph,

so that no two links sharing a vertex are of the same color, can be expressed as an integral over fermionic variables. We find two such integral representations: one that works for planar lattices only, and the other for non-planar graphs. Both of these integrals are amenable to field theory techniques.

One motivation for our study is as a controlled test of vector-like large- $N$  limits so common in condensed matter physics and high-energy physics.

## 2 Integral representation of the general dimer problem

We begin by describing our route to discovering Samuel's integral representation of the general dimer problem. Consider the following integral, associated with a graph  $\Gamma$ :

$$Z_1(\Gamma) \equiv \int D(\tilde{\eta}, \eta) e^{\sum_{\langle ij \rangle} A_{ij} \eta_i \tilde{\eta}_i \eta_j \tilde{\eta}_j} . \quad (2.1)$$

In this expression,  $(\eta_i, \tilde{\eta}_i)$  are two grassmann variables on each site of the graph  $\Gamma$ .

$$A_{ij} = \begin{cases} 1, & \text{if } ij \text{ is an edge of } \Gamma \\ 0, & \text{else} \end{cases} \quad (2.2)$$

is an unsigned adjacency matrix of  $\Gamma$ .  $\langle ij \rangle$  denotes an edge of  $\Gamma$  connecting sites  $i$  and  $j$ . In this paper, we do not use the Einstein summation convention for the site indices. The integration measure is

$$D(\tilde{\eta}, \eta) \equiv \prod_i (d\tilde{\eta}_i d\eta_i) . \quad (2.3)$$

We assume  $\Gamma$  has an even number of sites, since otherwise  $Z_1 = 0$ .

The partition function (2.1) counts the number of perfect matchings of the graph  $\Gamma$ . This is the number of ways of placing dimers on the edges of  $\Gamma$  such that each lattice site is paired with only one dimer. We can see this by doing the integral over the  $\tilde{\eta}$ s:

$$Z_1(\Gamma) = \int D\eta \text{Pf}_{ij} (A_{ij} \eta_i \eta_j) . \quad (2.4)$$

The argument of the Pfaffian is an antisymmetric  $2n \times 2n$  matrix in the  $ij$  indices, where  $2n$  is the number of sites of the graph  $\Gamma$ . Using the definition of the Pfaffian of a  $2n \times 2n$  antisymmetric matrix as

$$\text{Pf}_{ij}(M_{ij}) = C_n \sum_{\sigma \in S_{2n}} (-1)^\sigma M_{\sigma_1 \sigma_2} M_{\sigma_3 \sigma_4} \cdots M_{\sigma_{2n-1} \sigma_{2n}} \quad (2.5)$$

(where  $(-1)^\sigma$  is the sign of the permutation, and  $C_n \equiv \frac{1}{2^n n!}$ ) we can write  $Z_1$  as

$$Z_1(\Gamma) = C_n \int D\eta \sum_{\sigma \in S_{2n}} (-1)^\sigma \prod_{a=1}^n (A_{\sigma_{2a-1} \sigma_{2a}} \eta_{\sigma_{2a-1}} \eta_{\sigma_{2a}}) \quad (2.6)$$

$$= C_n \sum_{\sigma \in S_{2n}} \prod_{a=1}^n (A_{\sigma_{2a-1} \sigma_{2a}}) (-1)^\sigma \underbrace{\int D\eta \prod_{a=1}^n (\eta_{\sigma_{2a-1}} \eta_{\sigma_{2a}})}_{=(-1)^\sigma} \quad (2.7)$$

$$= \frac{1}{2^n n!} \sum_{\sigma \in S_{2n}} \prod_{a=1}^n (A_{\sigma_{2a-1} \sigma_{2a}}) . \quad (2.8)$$

This is manifestly the number of dimer coverings of the graph  $\Gamma$ . (The factor of  $\frac{1}{2^n n!}$  cancels the overcounting from swapping  $\sigma_{2a-1} \leftrightarrow \sigma_{2a}$  and swapping the labels on the  $n$  dimers.) Thus

$$Z_1(\Gamma) = \int D(\tilde{\eta}, \eta) e^{\sum_{(ij)} A_{ij} \eta_i \tilde{\eta}_i \eta_j \tilde{\eta}_j} = \text{Hf}(A), \quad (2.9)$$

the number of perfect matchings of a graph  $\Gamma$  is  $\text{Hf}(A)$ , the Haffnian of its adjacency matrix. Note that the Haffnian is not a linear algebra object, in that it does not behave well under basis transformations.

Interestingly, Kasteleyn showed that, if one considers planar lattices, the dimer tiling problem reduces to evaluating the pfaffian of the so called Kasteleyn matrix [1]. This is the signed adjacency matrix  $\tilde{A}$ , whose edges are oriented so that every face of the graph  $\Gamma$  has an odd number of clockwise oriented edges:

$$\tilde{A}_{ij} = \begin{cases} 1, & \text{if } ij \text{ is an edge of } \Gamma \text{ and } i \text{ points to } j \\ -1, & \text{if } ij \text{ is an edge of } \Gamma \text{ and } j \text{ points to } i \\ 0, & \text{else.} \end{cases} \quad (2.10)$$

We can summarize these findings as

$$\text{Dimer coverings} = \text{Hf}(A) \stackrel{\text{planar}}{=} \text{Pf}(\tilde{A}), \quad (2.11)$$

where the last equality is only true if the graph is planar and one can find the Kasteleyn matrix. It is interesting to note that the Kasteleyn matrix can be regarded as a discretization of the 2d Dirac operator. The pfaffian is a linear algebra object.

Quite generally, we could also include monomers in our partition function. If we wish to include a fugacity for monomers in the integral, we can modify it to

$$Z_1(\Gamma, x) \equiv \int D(\tilde{\eta}, \eta) e^{\sum_i x_i \eta_i \tilde{\eta}_i + \sum_{\langle ij \rangle} A_{ij} \eta_i \tilde{\eta}_i \eta_j \tilde{\eta}_j} . \quad (2.12)$$

Pulling down a power of  $x_i$  from the action removes the site  $i$  from the dimer coverings.

**Schwinger-Dyson equation.** The following line of thought gives an independent proof of the correctness of the non-gaussian grassmann integral representation for the monomer-dimer problem. Consider the following Schwinger-Dyson equation:

$$0 = \int D(\tilde{\eta}, \eta) \frac{\partial}{\partial \eta_i} \left( \eta_i e^{\sum_i x_i \eta_i \tilde{\eta}_i + \sum_{\langle ij \rangle} A_{ij} \eta_i \tilde{\eta}_i \eta_j \tilde{\eta}_j} \right) \quad (2.13)$$

$$= Z_1(\Gamma, x) - x Z_1(\Gamma - i, x) - \sum_j A_{ij} Z_1(\Gamma - i - j, x). \quad (2.14)$$

Here  $Z(\Gamma - \dots, x)$  means the partition function with the indicated ... removed from the graph. Each term can be interpreted as follows: The first term is all possible configurations of the graph  $\Gamma$ . The second term is all configurations with a monomer at site  $i$ . The third term is all configurations where a dimer ends at site  $i$ .

In fact, equation (2.14) is the main tool used by Heilmann and Lieb [6] to demonstrate the absence of a phase transition in this model at finite monomer fugacity. They show that the zeros of the partition function, as a function of the complex fugacity, all lie on the imaginary axis. And thus, the only value where a phase transition can occur is at  $x = 0$ .

**Parton construction.** The integrand of  $Z_1(\Gamma, x)$  has a local invariance under transformations of  $\eta, \tilde{\eta}$  that preserve the product  $\eta \tilde{\eta}$ . It is tempting to interpret the integral as arising from a parton decomposition of the following formal integral.

Define real ‘even grassmann variables’  $\zeta_i$ , satisfying the algebra

$$\zeta_i \zeta_j = \zeta_j \zeta_i, \quad \zeta_i^2 = 0. \quad (2.15)$$

We *define* integrals over such variables by the same condition as for odd grassmann integrals:

$$\int d\zeta \zeta = 1, \quad \int d\zeta 1 = 0. \quad (2.16)$$

Functions of  $\zeta$  are defined by Taylor expansion, *e.g.*  $e^\zeta = 1 + \zeta$ . With these definitions, the monomer-dimer tiling partition sum can be expressed as

$$Z_1(\Gamma, x) = \int \prod_{i=1}^n d\zeta_i e^{\sum_{\langle ij \rangle} \zeta_i A_{ij} \zeta_j + \sum_i x_i \zeta_i} \quad (2.17)$$

Now we apply the parton construction to these  $\zeta$  variables, by writing them (at each site) as a product of two ordinary grassmann variables

$$\zeta_i = \eta_i \tilde{\eta}_i. \quad (2.18)$$

One can check that the grassmann algebra implies the algebra (2.15). As with any parton construction, this decomposition comes with a gauge redundancy: any transformation of  $\eta, \tilde{\eta}$  that preserves  $\zeta = \eta \tilde{\eta}$  is a redundancy of this description that does not act on the physical degrees of freedom. Regarding  $\tilde{\eta}$  as the conjugate of  $\eta$ , *i.e.*  $\tilde{\eta} \equiv \eta^\dagger$ , we can see that there is a large gauge redundancy. Each site of the graph  $\Gamma$  has an on-site  $U(1)$ , given by

$$\eta_i \rightarrow e^{i\theta_i} \eta_i, \quad \tilde{\eta}_i \rightarrow e^{-i\theta_i} \tilde{\eta}_i. \quad (2.19)$$

This gauge redundancy will become crucial later on, as we will check in section §4.

### 3 Dimer piling problems

The grassmann integral representation for the general dimer problem is a strongly interacting field theory. A time-honored approach to such problems is to modify the problem to conjure a small parameter in which to expand. With this in mind, let’s contemplate the extension to  $N$  colors. That is, instead of a single pair of grassmann

| Colorings |  | Invariance                           |
|-----------|--|--------------------------------------|
| Type A    | $V_A = A_{ij} \eta_i^\alpha \tilde{\eta}_i^\alpha \eta_j^\beta \tilde{\eta}_j^\beta$ | $U(N, \mathbb{C})^{n_s}$             |
| Type B    | $V_B = A_{ij} \eta_i^\alpha \tilde{\eta}_i^\beta \eta_j^\alpha \tilde{\eta}_j^\beta$ | $O(N, \mathbb{C}) \times U(1)^{n_s}$ |
| Type C    | $V_C = A_{ij} \eta_i^\alpha \tilde{\eta}_i^\beta \eta_j^\beta \tilde{\eta}_j^\alpha$ | $U(N, \mathbb{C}) \times U(1)^{n_s}$ |
| Type D    | $V_D = A_{ij} \eta_i^\alpha \eta_i^\beta \tilde{\eta}_j^\beta \tilde{\eta}_j^\alpha$ | $U(N, \mathbb{C})$                   |

**Table 1:** The possible colorings of the dimer model. Models *A* through *C* reduce to the dimer tiling problem when  $N \rightarrow 1$ . We've written the invariance group of the model on a generic graph. On special graphs there can be an enhancement (for example, model B on a bipartite lattice has the same symmetry as model C).

variables at each site of the graph  $\Gamma$ , we have variables  $(\eta_i^\alpha, \tilde{\eta}_i^\alpha)_{\alpha=1..N, i \in \Gamma}$ . We will call the index  $\alpha$  a color index.

Consider the following partition function:

$$Z_N(\Gamma, x, V) \equiv \int D(\tilde{\eta}, \eta)^\alpha e^{\sum_i x \eta_i^\alpha \tilde{\eta}_i^\alpha + \frac{1}{N} V(\eta_i^\alpha, \tilde{\eta}_i^\beta, \eta_j^\rho, \tilde{\eta}_j^\sigma)}, \quad (3.1)$$

where the integration measure is

$$D(\tilde{\eta}, \eta)^\alpha \equiv \prod_{i, \alpha} (d\tilde{\eta}_i^\alpha d\eta_i^\alpha) . \quad (3.2)$$

We have in the action (3.1) two terms. The first term is a Gaussian term describing colorful monomers. The second term is the potential  $V$ , which could, in principle, describe different kinds of colorful objects, such as dimers, trimers, wedges, or sphinxes. In this paper, we will focus on quartic interactions, which represent colorful dimers. Note that a factor of  $1/N$  is placed in front of the potential. As we will see later on, this factor is designed to make the free energy extensive in  $N$ .

Four distinct possibilities for the potential  $V$  exist, which we will label from *A* to *D*. All of these possibilities can be organized by symmetry, as showcased in table 1. However, we could also require that when the number of colors  $N$  is set to 1, the model reduces to the usual monomer-dimer problem on  $\Gamma$ . This constrains the number of possibilities to three, *A* through *C*. If we further demand that the weights of the associated combinatorial problem are positive on an arbitrary graph, we are left with models *A* and *B*.



with

$$S_0 = \frac{1}{N} \sum_{\langle ij \rangle} A_{ij} \eta_i^\alpha \tilde{\eta}_i^\alpha \eta_j^\beta \tilde{\eta}_j^\beta. \quad (3.7)$$

Note that because of the couplings between the colors  $\alpha \neq \beta$ , this is not just a decoupled stack of  $N$  dimer problems:  $Z_N^A \neq (Z_1)^N$ . The right-hand side here counts multi-dimer tilings of  $\Gamma$  with each site covered by exactly  $N$  dimers. For example, for  $N = 2$ , any collection of closed loops is allowed, including loops that backtrack across a link. Such a collection of closed loops can be regarded as (the symmetric difference of) an arbitrary pair of dimer tilings (as defined in e.g. [15]). But we must specify the measure with which such configurations are counted.

To see what combinatorial problem we have defined, observe that the only nonzero contributions to  $Z_N^A$  arise from integrals of the form

$$\int \prod_{\alpha} d\tilde{\eta}_i^\alpha d\eta_i^\alpha \left( \sum_{\alpha} \eta_i^\alpha \tilde{\eta}_i^\alpha \right)^N = N! \quad (3.8)$$

for each site  $i$ .

$$Z_N^A(\Gamma) = \int D(\tilde{\eta}, \eta)^\alpha \prod_{\ell} e^{S_{\ell}} \quad (3.9)$$

$$= \int D(\tilde{\eta}, \eta)^\alpha \prod_{\ell} \left( \sum_{n_{\ell}=0}^{\infty} \frac{1}{n_{\ell}!} S_{\ell}^{n_{\ell}} \right) \quad (3.10)$$

Here the product is over (undirected) links of  $\Gamma$  and  $S_{\langle ij \rangle} \equiv \frac{1}{N} A_{ij} \eta_i^\alpha \tilde{\eta}_i^\alpha \eta_j^\beta \tilde{\eta}_j^\beta$ .

In order to get a nonzero contribution to the integral over the grassmanns at site  $i$  in (3.10), the  $n_{\ell}$  must satisfy

$$\sum_{\langle ij \rangle} n_{ij} = N, \quad (3.11)$$

where the notation  $\sum_{\langle ij \rangle}$  means sum over  $j$  with  $i$  fixed. This constraint can be regarded as a Gauss law for the  $U(1)^n$  redundancy of model A. (A similar constraint will appear in models B and C, which also have such a  $U(1)^n$  gauge redundancy.) Below, this will be interpreted as a local number conservation of a class of ‘‘particles’’.

Using (3.8) at each site, the result is

$$Z_N^A(\Gamma) = (N!)^{n_s} \sum_{\text{dimer tilings}} \prod_{\ell} \frac{1}{N^{n_{\ell}} (n_{\ell})!} \quad (3.12)$$

where  $n_s$  is the number of sites of the graph  $\Gamma$ , and the sum over dimer pilings indicates a non-negative integer for each link, satisfying (3.11). In a nonzero contribution, we interpret  $n_\ell$  as the number of dimers on the link  $\ell$ . We can interpret the factor of  $\frac{1}{(n_\ell)!}$  as indicating that the dimers are *indistinguishable*.

In the same spirit, we can define “the model- $B$  dimer  $N$ -piling problem on a graph  $\Gamma$ ” as the integral with  $V = V_B$ :

$$Z_N^B(\Gamma) = \int D(\tilde{\eta}, \eta)^\alpha e^{S_0} \quad (3.13)$$

with

$$S_0 = \frac{1}{N} \sum_{\langle ij \rangle} A_{ij} \eta_i^\alpha \tilde{\eta}_i^\beta \eta_j^\alpha \tilde{\eta}_j^\beta, \quad (3.14)$$

where we now instead contract the color indices  $\eta_i^\alpha$  with  $\eta_j^\alpha$ , and  $\tilde{\eta}_i^\beta$  with  $\tilde{\eta}_j^\beta$ .

It is worth emphasizing the effect of this choice of interaction: it decouples the  $\eta$  from the  $\tilde{\eta}$  such that each variable can be colored *independently*. That is, for every piling  $\mathcal{C}$  coming from expanding (3.13), the integral factorizes and the variables are colorwise independent.

For example, consider tiling the two-site open chain. The only term contributing to the partition comes from filling its link  $\langle ij \rangle$  with  $N$  dimers:

$$Z_N^B(\Gamma) = \int D(\tilde{\eta}, \eta)^\alpha \frac{1}{N!} \left( \frac{1}{N} \sum_{\alpha, \beta} \eta_i^\alpha \tilde{\eta}_i^\beta \eta_j^\alpha \tilde{\eta}_j^\beta \right)^N \quad (3.15)$$

$$= \int D(\tilde{\eta}, \eta)^\alpha \frac{(-1)^N}{N! N^N} \left( \sum_\alpha \eta_i^\alpha \eta_j^\alpha \right)^N \left( \sum_\beta \tilde{\eta}_i^\beta \tilde{\eta}_j^\beta \right)^N = \frac{(N!)^2}{N^N N!} \quad (3.16)$$

We get  $N!$  from each integral, one from piling the  $\eta$  and the other from the  $\tilde{\eta}$ .

How can we interpret the resulting factor in (3.16)? We see that pilings  $\mathcal{C}$  of model  $B$ , define the same piling structure in the  $\eta$ 's and the  $\tilde{\eta}$ 's. In other words, it defines copies  $\mathcal{C}_\eta$  and  $\mathcal{C}_{\tilde{\eta}}$  living on the variables  $\eta$  and  $\tilde{\eta}$  respectively. At each of these copies, we still need to satisfy that, at each site, there are  $N$  different colorful grassmannans. As a consequence, the total factor one gets is the number of ways of arranging colorful  $\eta$ -dimers in  $\mathcal{C}_\eta$  times the number of ways of arranging colorful  $\tilde{\eta}$ -dimers in  $\mathcal{C}_{\tilde{\eta}}$ , satisfying such constraint. But since these are strict copies, this equals the square of the number of ways of coloring the piling  $\mathcal{C}$ .

These facts, combined with the condition (3.11), lead to

$$Z_N^B(\Gamma) = \sum_{\text{dimer pilings } \mathcal{C}=\{n_\ell\}} \prod_{\ell} \frac{1}{N^{n_\ell} (n_\ell)!} \left( \# \begin{array}{c} \text{ways of coloring} \\ \text{dimer piling } \mathcal{C} \end{array} \right)^2, \quad (3.17)$$

where now it gets a factor depending on the number of ways of distributing the colorful dimers, which is squared as we are coloring  $\eta$ 's and  $\tilde{\eta}$ 's independently.

We also see in (3.16) that negative signs appear from permuting the grassmann variables. This could imply that different dimer pilings come with relative sign factors, leading to a sum of alternating sign terms in the partition function. This is not the case for model *B*: all terms in the expansion do come with the same positive sign, as is manifest in (3.17). In the appendix A, we give a graphical method to understand how the signs from the grassmann variables conspire to cancel out in model *B*, unlike in model *C*.

Lastly, we define the “the model-*C* dimer  $N$ -piling problem on a graph  $\Gamma$ ” as the integral with  $V = V_C$ :

$$Z_N^C(\Gamma) = \int D(\tilde{\eta}, \eta)^\alpha e^{S_0} \quad (3.18)$$

with

$$S_0 = \frac{1}{N} \sum_{\langle ij \rangle} A_{ij} \eta_i^\alpha \tilde{\eta}_i^\beta \eta_j^\beta \tilde{\eta}_j^\alpha, \quad (3.19)$$

which defines the combinatorial problem over the two copies  $\mathcal{C}_\eta$  and  $\mathcal{C}_{\tilde{\eta}}$  of a piling  $\mathcal{C}$ , just as in model *B*, but contracts the color indices  $\eta_i^\alpha$  with  $\tilde{\eta}_j^\alpha$ , and  $\tilde{\eta}_i^\beta$  with  $\eta_j^\beta$ .

Model *C* is indeed very much related to model *B*. As a matter of fact, they are the same on a bipartite graph. This can be seen by substiting in (3.13) the following transformation on one of the two sublattices:  $(\eta_i^\alpha, \tilde{\eta}_i^\alpha) \rightarrow (\tilde{\eta}_i^\alpha, -\eta_i^\alpha)$ , which leads to (3.18). Therefore, on a bipartite lattice, the invariance group of model *B* is enlarged to that of  $C^1$ . Under this condition, the partition function  $Z_N^C$  is just (3.17).

---

<sup>1</sup>The explicit expression for the  $U(N)$  symmetry of model *B* on a bipartite graph is

$$\begin{aligned} \eta_A^\alpha &\rightarrow U^{\alpha\beta} \eta_A^\beta, & \eta_B^\alpha &\rightarrow (U^\dagger)^{\alpha\beta} \eta_B^\beta, \\ \tilde{\eta}_A^\alpha &\rightarrow (U^\dagger)^{\alpha\beta} \tilde{\eta}_A^\beta, & \tilde{\eta}_B^\alpha &\rightarrow U^{\alpha\beta} \tilde{\eta}_B^\beta, \end{aligned}$$

where the subscript *A/B* refers to the two sublattices.

However, on non-bipartite graphs, these two models are not the same: the argument forbidding negative sign contributions fails for model  $C$ , and negative terms do appear. This in turn means that we need to find out how do type- $C$  dimers color the two copies of the piling  $\mathcal{C}$ , which reduces to model B in a bipartite graph. This is not an easy task using integrals, but straightforward using the graphical methods of Appendix A. For that reason, we present the partition function of model  $C$  here and leave the explanation in the appendix.

$$Z_N^C(\Gamma) = \sum_{\text{dimer pilings } \mathcal{C}=\{n_\ell\}} \prod_{\ell} \frac{(-1)^{C_\ell}}{N^{n_\ell} (n_\ell)!} \left( \# \text{ ways of coloring } \mathcal{C}_\eta \text{ and } \mathcal{C}_{\bar{\eta}} \text{ with type-}C \text{ dimers} \right). \quad (3.20)$$

One can add a monomer fugacity in any model, the same way as for  $N = 1$ , by perturbing the action by an on-site quadratic term

$$S[\eta] = \sum_{i,\alpha} x_i \eta_i^\alpha \tilde{\eta}_i^\alpha + S_0. \quad (3.21)$$

The way this monomer term interplays with the dimer term differs when considering model  $A$  vs  $B/C$ . For model  $A$ , at the cost of a factor of  $x_i$ , this allows the site  $i$  to be covered by one fewer dimer. But for the other models, this will remove one site of the same color  $\alpha$  at each  $\mathcal{C}_\eta$  and  $\mathcal{C}_{\bar{\eta}}$ .

## 4 Large- $N$ analysis

In this section, we will make use of large- $N$  field theory methods. We begin by presenting the partition function for the different types of coloring, and introduce an auxiliary field  $\phi_{ij}$  for each of them. We shall denote this field  $\phi_{ij}$  as a link field since it lives on the links  $\langle ij \rangle$  of the graph. An effective action of these link fields is obtained after integrating out the original degrees of freedom, and at large  $N$  is amenable to saddle point techniques. We study the resulting mean-field equations and find the dominant saddle configurations. We consider fluctuations around the saddle to get an effective partition function and its free energy density.

In the subsequent subsection, we will also study the partition function using a diagrammatic expansion, and compare the result with the saddle point calculation. We identify the leading connected diagrams for each coloring, and resum them to find the corresponding free energy density.

**Model A.** Consider the first generalization to  $N$  colors, which we called coloring type  $A$ . Let us perform a Hubbard-Stratonovich decoupling of the quartic term by introducing auxiliary link variables  $\phi_{ij}$ :

$$e^{\frac{1}{N} \sum_{\langle ij \rangle} A_{ij} \eta_i^\alpha \tilde{\eta}_i^\alpha \eta_j^\beta \tilde{\eta}_j^\beta} = \int D(\phi, \phi^*) e^{\sum_{\langle ij \rangle} -N \phi_{ij} \phi_{ij}^* + \sqrt{A_{ij}} (\eta_i^\alpha \tilde{\eta}_i^\alpha \phi_{ij} + \eta_j^\alpha \tilde{\eta}_j^\alpha \phi_{ij}^*)}. \quad (4.1)$$

After integrating out the  $\eta, \tilde{\eta}$  variables, we can rewrite the partition function as a path integral over the field  $\phi_{ij}$ ,

$$Z_N^A(\Gamma, x) = \int D(\phi, \phi^*) e^{-N S_A[\phi, \phi^*]}, \quad (4.2)$$

where the effective action  $S_A[\phi, \phi^*]$  is

$$S_A[\phi, \phi^*] = \sum_{\langle ij \rangle} \phi_{ij} \phi_{ij}^* - \sum_i \ln \left| x + \sum_{\langle ij \rangle} \sqrt{A_{ij}} (\phi_{ij} + \phi_{ji}^*) \right|. \quad (4.3)$$

By solving its equation of motion in (4.1), we can relate  $\phi$  to an expectation value of monomers at a site. This is because, at the saddle point,  $\phi_{ij}^{\text{saddle}} = \frac{1}{N} \sum_\alpha (\eta_i^\alpha \tilde{\eta}_i^\alpha + \eta_j^\alpha \tilde{\eta}_j^\alpha)$ . Model A has a time-reversal symmetry under which  $\eta \leftrightarrow \tilde{\eta}, \phi_{ij} \rightarrow \phi_{ij}^* = \phi_{ji}$  which shows that the action is real and all configurations contribute with positive weight.

**Model B.** Next, consider the second generalization, which we named coloring type  $B$ . We introduce an auxiliary Hubbard-Stratonovich link field  $\phi_{ij}$  to decouple the type- $B$  interaction:

$$e^{\frac{1}{N} \sum_{\langle ij \rangle} A_{ij} \eta_i^\alpha \tilde{\eta}_i^\beta \eta_j^\alpha \tilde{\eta}_j^\beta} = \int D(\phi, \phi^*) e^{\sum_{\langle ij \rangle} -N \phi_{ij} \phi_{ij}^* + \sqrt{A_{ij}} (\eta_i^\alpha \eta_j^\alpha \phi_{ij}^* - \tilde{\eta}_i^\alpha \tilde{\eta}_j^\alpha \phi_{ij})}. \quad (4.4)$$

Doing the integral over the  $\eta, \tilde{\eta}$  fields, one gets the type- $B$  partition function as a integral over the complex field  $\phi_{ij}$ ,

$$Z_N^B(\Gamma, x) = \int D(\phi, \phi^*) e^{-N S_B[\phi, \phi^*]}, \quad (4.5)$$

where the effective action  $S_B[\phi, \phi^*]$  is

$$S_B[\phi, \phi^*] = \sum_{\langle ij \rangle} \phi_{ij} \phi_{ij}^* - \frac{1}{2} \text{tr} \ln \begin{pmatrix} -B(\phi^*) & -x\mathbb{1} \\ x\mathbb{1} & B(\phi) \end{pmatrix}, \quad (4.6)$$

and the block matrix  $B$  is

$$B(\phi) = \sum_{\langle ij \rangle} \phi_{ij} (|i\rangle\langle j| - |j\rangle\langle i|). \quad (4.7)$$

In comparison with model  $A$ , this model at the saddle point of (4.4) is related to the dimer density at a link according to  $\phi_{ij}^{\text{saddle}} = \frac{1}{N} \sum_{\alpha} \eta_i^{\alpha} \eta_j^{\alpha}$ . Importantly, this suggests that  $\phi$  transforms under the gauge redundancy in (2.19) as  $\phi_{ij} \rightarrow e^{i(\theta_i + \theta_j)} \phi_{ij}$ , making  $\phi_{ij}$  a gauge non-invariant variable.

Model  $B$  also has a time-reversal symmetry under which  $\eta \leftrightarrow \tilde{\eta}$ ,  $\phi_{ij} \rightarrow \phi_{ij}^*$  which shows that the action is real and all configurations contribute with positive weight.

**Model C.** Lastly, we implement the decoupling for model  $C$ . The Hubbard-Stratonovich transformation that trades the quartic interaction is:

$$e^{\frac{1}{N} \sum_{\langle ij \rangle} A_{ij} \eta_i^{\alpha} \tilde{\eta}_i^{\beta} \eta_j^{\beta} \tilde{\eta}_j^{\alpha}} = \int D(\phi, \phi^*) e^{\sum_{\langle ij \rangle} -N \phi_{ij} \phi_{ij}^* + \sqrt{A_{ij}} (\eta_i^{\alpha} \tilde{\eta}_j^{\alpha} \phi_{ij}^* + \tilde{\eta}_i^{\alpha} \eta_j^{\alpha} \phi_{ij})}. \quad (4.8)$$

After integrating out the original variables, the partition function for type- $C$  becomes

$$Z_N^C(\Gamma, x) = \int D(\phi, \phi^*) e^{-N S_C[\phi, \phi^*]}, \quad (4.9)$$

where the effective action  $S_C[\phi, \phi^*]$  is

$$S_C[\phi, \phi^*] = \sum_{\langle ij \rangle} \phi_{ij} \phi_{ij}^* - \frac{1}{2} \text{tr} \ln \begin{pmatrix} 0 & C(\phi, \phi^*) \\ -C^T(\phi, \phi^*) & 0 \end{pmatrix}, \quad (4.10)$$

and the block matrix  $C$  is

$$C(\phi, \phi^*) = - \sum_i x |i\rangle\langle i| + \sum_{\langle ij \rangle} (-\phi_{ij}^* |i\rangle\langle j| + \phi_{ij} |j\rangle\langle i|). \quad (4.11)$$

The solution of the equations of motion in (4.8) lead to  $\phi_{\text{saddle}} = \frac{1}{N} \sum_{\alpha} \eta_i^{\alpha} \tilde{\eta}_j^{\alpha}$ . As in model  $B$ , we see that we can similarly interpret the field as the dimer density in the link.

Model  $C$  does *not* have a time-reversal symmetry and indeed the action  $S_C$  is not real in general. We will see below that (on a non-bipartite graph) some configurations of model  $C$  contribute with negative weight.

## 4.1 Saddle point analysis

The large- $N$  limit of the  $(\eta, \tilde{\eta})$  theory (3.1) is the semiclassical limit of the  $(\phi, \phi^*)$  fields introduced above. Thus, in the limit  $N \rightarrow \infty$ , the partition function is determined by the configuration that makes the action stationary:

$$\left. \frac{\delta S}{\delta \phi_{ij}} \right|_{\phi_0, \phi_0^*} = \left. \frac{\delta S}{\delta \phi_{ij}^*} \right|_{\phi_0, \phi_0^*} = 0. \quad (4.12)$$

With the mean field determined, we proceed to expand the functional in fluctuations around  $(\phi_0)_{ij}$ . We will denote such fluctuations as  $\tilde{\phi}_{ij} = \phi_{ij} - (\phi_0)_{ij}$ , and  $\tilde{\phi}_{ij}^* = \phi_{ij}^* - (\phi_0^*)_{ij}$ . The expansion of the action around mean field is thus:

$$S[\phi, \phi^*] = S_0 + S^{(1)}[\tilde{\phi}, \tilde{\phi}^*] + S^{(2)}[\tilde{\phi}, \tilde{\phi}^*] + \dots, \quad (4.13)$$

where the first term  $S_0 \equiv S[\phi_0, \phi_0^*]$  is an overall constant multiplying the partition function  $e^{-NS_0} = Z_0$ . The second term  $S^{(1)}$ , linear in the fields, is equal to zero as we are expanding around the saddle. The third term  $S^{(2)}$ , quadratic in the fields, is the second-order fluctuation and corresponds to one-loop corrections:

$$S^{(2)}[\tilde{\phi}, \tilde{\phi}^*] = \frac{1}{2} \left. \frac{\delta^2 S}{\delta \phi_{ij} \delta \phi_{nm}} \right|_{\phi_0, \phi_0^*} \tilde{\phi}_{ij} \tilde{\phi}_{nm} + \frac{1}{2} \left. \frac{\delta^2 S}{\delta \phi_{ij}^* \delta \phi_{nm}^*} \right|_{\phi_0, \phi_0^*} \tilde{\phi}_{ij}^* \tilde{\phi}_{nm}^* + \left. \frac{\delta^2 S}{\delta \phi_{ij} \delta \phi_{nm}^*} \right|_{\phi_0, \phi_0^*} \tilde{\phi}_{ij} \tilde{\phi}_{nm}^*. \quad (4.14)$$

One can then get the effective partition function after integrating over these Gaussian fluctuations,

$$Z_{\text{eff}} = e^{-NS_0} \int D(\tilde{\phi}, \tilde{\phi}^*) e^{-NS^{(2)}[\tilde{\phi}, \tilde{\phi}^*]} = e^{-NS_0 - N^0 S_1}, \quad (4.15)$$

which defines the free energy density  $f = -\lim_{n_s \rightarrow \infty} \frac{1}{n_s} \ln Z_{\text{eff}}$ . Notice that  $Z_{\text{eff}}$  omits the terms in the free energy that go like negative powers of  $N$  coming from higher-loop contributions. At large  $N$ ,  $Z_{\text{eff}}$  counts the weighted monomer-dimer configurations described in §A. However, at finite  $N$ ,  $Z_{\text{eff}}$  is not necessarily an integer.

**Model A.** Taking the functional derivative of (4.3), we get

$$\frac{\delta S_A}{\delta \phi_{ij}} = \phi_{ij}^* - \frac{\sqrt{A_{ij}}}{x + \sum_{\langle ik \rangle} \sqrt{A_{ik}} (\phi_{ik} + \phi_{ki}^*)}, \quad \frac{\delta S_A}{\delta \phi_{ij}^*} = \phi_{ij} - \frac{\sqrt{A_{ji}}}{x + \sum_{\langle jk \rangle} \sqrt{A_{jk}} (\phi_{jk} + \phi_{kj}^*)}. \quad (4.16)$$

Equation (4.16) is a system of equations, which can be solved in principle, that highly depends on the graph we are considering. For simplicity, we restrict our attention to translation-invariant lattices, for which a spatially uniform solution is naturally the first guess to solve these equations. We shall see that indeed this configuration is free-energetically favorable and provides a stable extremum.

Using the homogeneous configuration as an ansatz in (4.12), we see that it is real ( $\phi_0 = \phi_0^*$ ) and equal to

$$\phi_0 = \frac{-x \pm \sqrt{x^2 + 4z}}{2z}, \quad (4.17)$$

where  $z$  is the coordination number.

We see that, in (4.17), two solutions exist. These two mean fields will dominate in different regimes. The positive root solution dominates when  $x > 0$ , while the negative root dominates when  $x < 0$ .

Let's give some examples. We start with the simplest one, the  $1D$  periodic chain. We can find its exact solution using transfer matrix methods and use it to compare it with our saddle point approach. We do this in Appendix B. As we already know the mean field, we will continue with the second-order fluctuations. And since we are dealing with translation invariant graphs, we can simplify (4.14) by going to Fourier space,

$$S_A^{(2)}[\tilde{\phi}, \tilde{\phi}^*] = \frac{1}{2} \sum_{p \in BZ} (\tilde{\phi}_p \ \tilde{\phi}_{-p}^*) \begin{pmatrix} 1 + e^{ip} \phi_0^2 & \phi_0^2 \\ \phi_0^2 & 1 + e^{-ip} \phi_0^2 \end{pmatrix} \begin{pmatrix} \tilde{\phi}_p^* \\ \tilde{\phi}_{-p} \end{pmatrix}. \quad (4.18)$$

and compute the free energy density

$$f_{1D} = N(\phi_0^2 - \ln|x + 2\phi_0|) - \frac{1}{2} \ln \left( \frac{2}{1 + \sqrt{1 - 4\phi_0^4}} \right). \quad (4.19)$$

Plots of the effective free energy density compared to the exact solution obtained by transfer matrix methods, for different number of colors  $N$ , are presented in Figure 1. As expected, exact solution (blue) and mean field plus one-loop corrections (green) become indistinguishable as we consider larger values of  $N$ . As first observed in [13], it also gives pretty good results for  $N = 1$ . Notice the sharp difference between odd/even number of colors. Series expansion around  $x = 0$  shows that for even colors the leading correction is  $x^2$  while for odd colors it is  $|x|$ .

We can do the same procedure for other translation invariant graphs. On any lattice, we can diagonalize the Gaussian fluctuations, find its spectrum, and get the

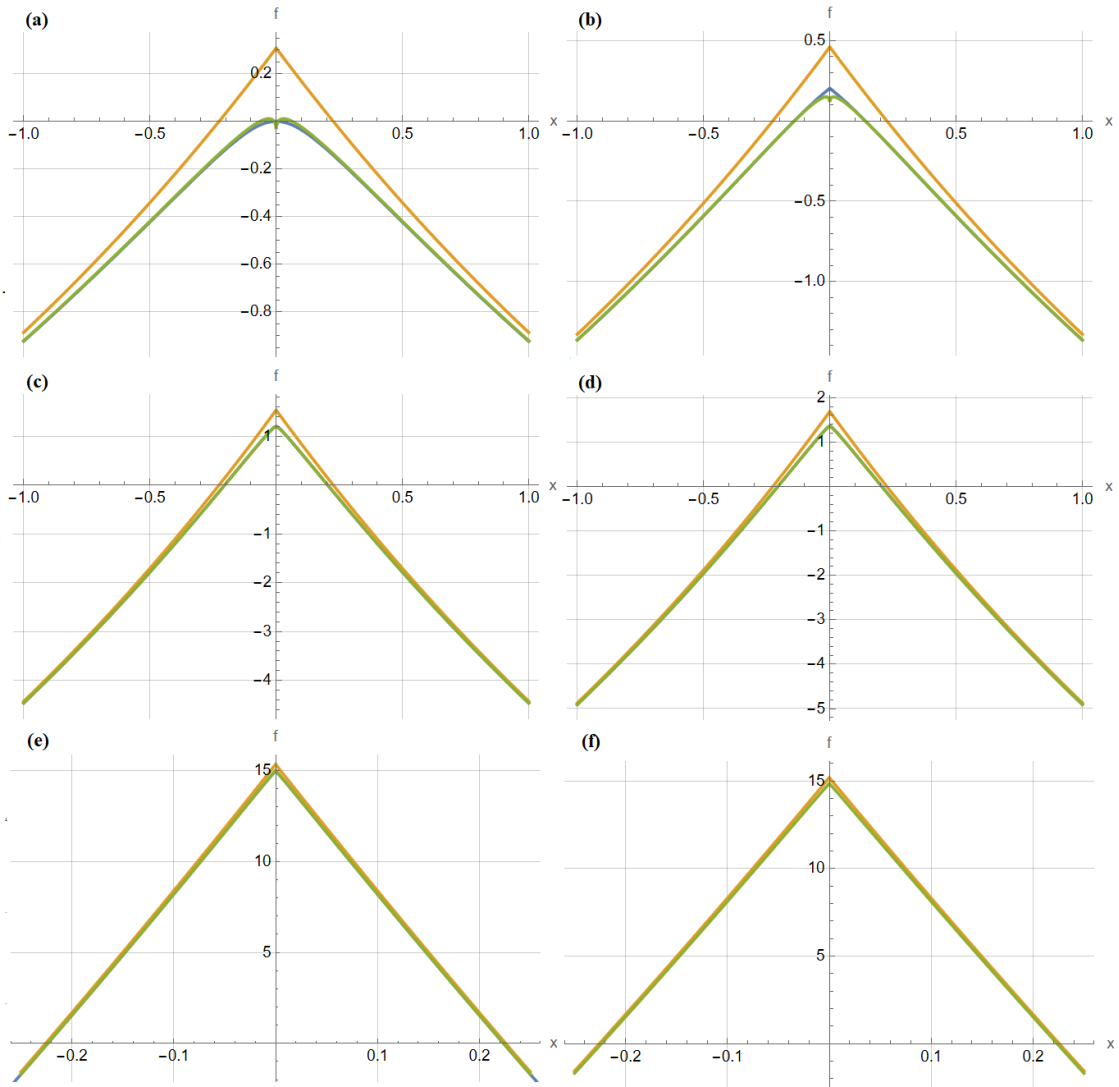


**Figure 1:**  $1D$ , type- $A$  free energy density  $f$  for the exact solution (blue), mean field (orange) and mean field including the one-loop correction (green) as a function of the coupling  $x$  for different number parity: evens (a)  $N = 2$ , (c)  $N = 10$ , (e)  $N = 100$ , and odds (b)  $N = 3$ , (d)  $N = 11$ , (f)  $N = 99$ . Even at small values of  $N$ , the effective free energy density (4.19) represents an extremely well-approximation of the exact solution.

effective free energy density. In particular, for a Bravais lattice with coordination

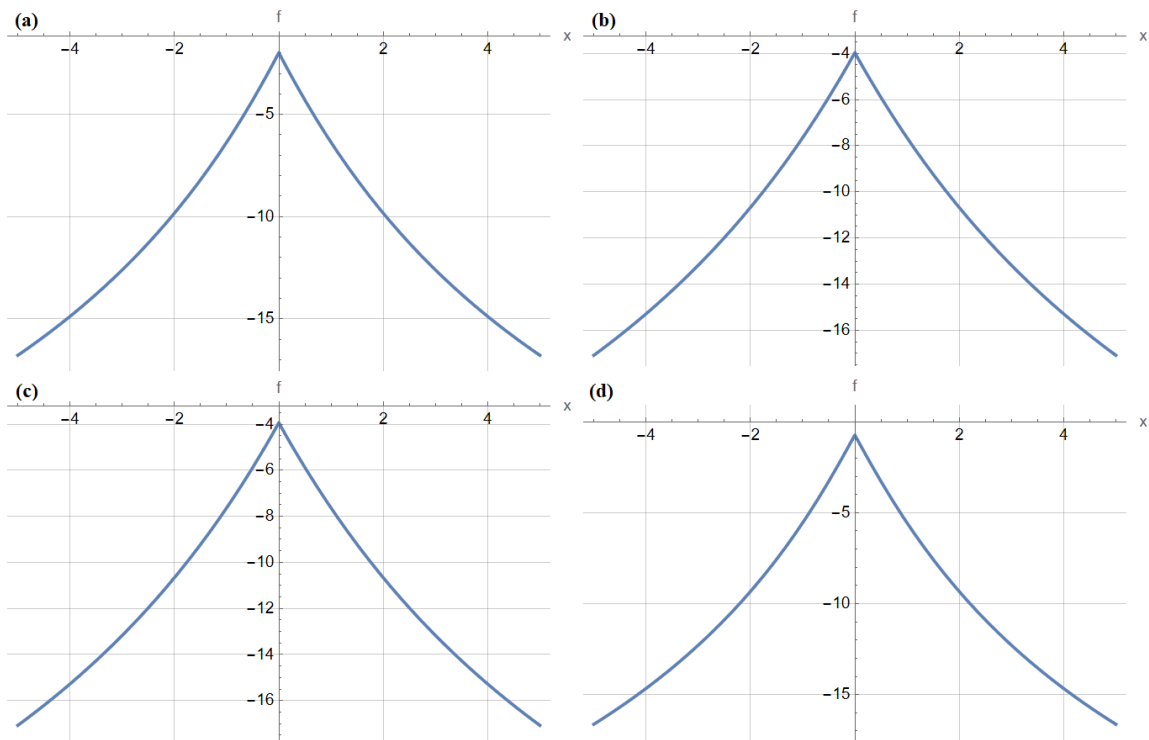


**Figure 2:** Type-A free energy density  $f_A$  for  $N = 10$  and different lattices. We consider Bravais lattices ((a) to (c)), which follow (4.20): (a) square lattice, (b) cubic lattice, (c) triangular lattice; but also (d) honeycomb lattice. As discussed, no phase transition occurs at finite  $x$ .

number  $z$ , we find that the free energy density is:

$$f_A = N \left( \frac{1}{2} z \phi_0^2 - \ln |x + z \phi_0| \right) + \frac{\nu_0}{2} \int_{BZ} \frac{d^d p}{(2\pi)^d} \ln \left( 1 + 2 \phi_0^2 \sum_i \cos(\vec{p} \cdot \hat{e}_i) \right), \quad (4.20)$$

where  $\nu_0$  is the unit cell volume, and  $\hat{e}_i$  are the primitive vectors. In Appendix C, we give the details of this calculation along with the generalization to the case with separate dimer fugacities for each link direction.

We note that when the monomer fugacity  $x \neq 0$ , the argument inside the logarithm is positive and thus, the uniform saddle point is stable. The free energy density is analytic in  $x$  away from  $x = 0$  and no phase transition occurs at finite monomer fugacity. Only in the pure dimer limit ( $x = 0$ ) does the argument of the logarithm vanish, and the free energy is singular, in agreement with Heilmann and Lieb when  $N = 1$ . For any  $N$ , the deformation to include different dimer fugacities for different

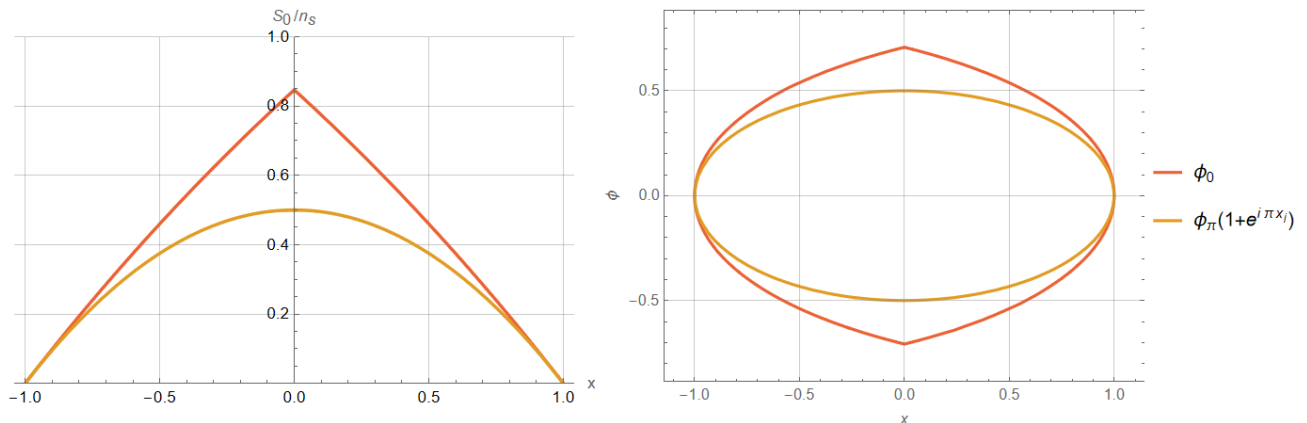


**Figure 3:** (a) Leading order term  $S_0$  over number of sites  $n_s$  in (4.15) of the 1D periodic chain for the homogeneous solution  $(\phi_0)_{ij} = \phi_0$  (red) and the textured solution  $(\phi_0)_{ij} = \phi_\pi(1 + e^{i\pi x_i})$  (orange). We see that the alternating mean field is energetically favorable for all values of  $x$ . (b) Gap equation solutions of the chain for the homogeneous  $\phi_0$  and alternating mean field  $\phi_\pi$ .

dimer directions also resolves the singularity (see Appendix C), as it does for  $N = 1$  [4, 5, 7].

**Model B.** Let's proceed with model *B* and begin by identifying the mean-field configurations of  $\phi$  for which the action is minimized.

The first guess would be to try a homogeneous solution, just like in the previous model. However, this solution to the mean-field equations is not the dominant saddle point. A detailed analysis of such constant ansatz is presented in Appendix C. Rather, a textured configuration that breaks translation symmetry will be energetically superior. This can be seen in figure 3 for the 1D periodic chain for example, where the textured configuration  $(\phi_0)_{ij} = \phi_\pi(1 + e^{i\pi x_i})$  provides a stable extremum as we will see. We shall call this configuration the alternating mean field.

Let's continue exploring the periodic chain. The first variation of the action (4.6) evaluated at such mean field leads to the gap equation,

$$\left. \frac{\delta S_B}{\delta \phi_{ij}} \right|_{\phi_\pi, \phi_\pi^*} = 2n_s \phi_\pi - \frac{4\phi_\pi}{x^2 + 4\phi_\pi^2} \sum_p \sin^2(p) = 0. \quad (4.21)$$

Solving (4.21), we get that either  $\phi_\pi = 0$  or  $\phi_\pi^2 = \frac{1}{4}(1 - x^2)$ . We note that the non-trivial solution only exists on the interval  $|x| < 1$ , while outside this interval  $\phi_\pi = 0$  is the only solution, as seen in figure 3.

Interestingly, this all means that a phase transition occurs at finite monomer fugacity: there exists a critical value  $x_c = \pm 1$  for which  $\phi$  starts to condense. We can understand this picture by remembering that  $\phi$  at the saddle was proportional to the number of dimers at a link of the graph. At small values of  $x$ , it is favorable to fully cover the graph with mostly dimers. As the monomer fugacity starts increasing in value, the number of sites covered by monomers increases, reducing the number of dimers per link, until it eventually reaches the critical point  $x = 1$  where the monomers are free.

We proceed next to calculate the second-order fluctuations (4.14) around the alternating mean field for  $|x| < x_c$ . This configuration  $\phi_\pi$  preserves translations by two lattice sites. Hence, we double the unit cell size and work in Fourier space to get

$$S_B^{(2)}[\tilde{\phi}, \tilde{\phi}^*] = \sum_{p \in (0, \frac{\pi}{2})} (\tilde{\phi}_p \tilde{\phi}_{p+\pi} \tilde{\phi}_{-p}^* \tilde{\phi}_{-p+\pi}^*) \begin{pmatrix} 1-x^2 & 0 & 2\phi_\pi^2 & 2\phi_\pi^2 \\ 0 & 1-x^2 & 2\phi_\pi^2 & 2\phi_\pi^2 \\ 2\phi_\pi^2 & 2\phi_\pi^2 & 1-x^2 & 0 \\ 2\phi_\pi^2 & 2\phi_\pi^2 & 0 & 1-x^2 \end{pmatrix} \begin{pmatrix} \tilde{\phi}_p^* \\ \tilde{\phi}_{p+\pi}^* \\ \tilde{\phi}_{-p} \\ \tilde{\phi}_{-p+\pi} \end{pmatrix}. \quad (4.22)$$

Yet, looking at its spectrum, this matrix is singular: it has zero-modes with zero eigenvalues for every value of  $p$ . This is a manifestation of the gauge redundancy  $\phi_{ij} \rightarrow e^{i(\theta_i + \theta_j)} \phi_{ij}$  of this model. Under the gauge transformation, the action (4.6) is invariant<sup>2</sup>.

To lift the gauge redundancy, we do gauge fixing, details of which are presented in appendix C. We present here the result for the free energy density

$$f_{1D} = \frac{N}{2}(1-x^2) - \frac{1}{4} \ln(8\pi N) + \frac{1}{2} \ln(1-x^2), \quad |x| < 1. \quad (4.25)$$

---

<sup>2</sup>The action  $S_B$  transforms as

$$S_B \rightarrow S'_B = \sum_{\langle ij \rangle} |\phi_{ij}|^2 - \frac{1}{2} \text{tr} \ln \begin{pmatrix} -\sum_{\langle ij \rangle} e^{-i(\theta_i + \theta_j)} \phi_{ij}^* (|i\rangle\langle j| - |j\rangle\langle i|) & -x\mathbb{1} \\ x\mathbb{1} & \sum_{\langle ij \rangle} e^{i(\theta_i + \theta_j)} \phi_{ij} (|i\rangle\langle j| - |j\rangle\langle i|) \end{pmatrix}, \quad (4.23)$$

which using the invariance property of the trace  $\text{tr}(A) = \text{tr}(U^\dagger A U)$  under the unitary transformation

$$U_\gamma = \begin{pmatrix} 0 & \sum_j e^{-i\theta_j} |j\rangle\langle j| \\ \sum_j e^{i\theta_j} |j\rangle\langle j| & 0 \end{pmatrix} \quad (4.24)$$

shows the action invariance  $S'_B = S_B$ .

Remarkably, we get a contribution proportional to  $\ln N$ . This is a product of the gauge fixing calculation and comes from the measure of the integral as shown in §C. The last term is actually singular at the transition point  $x = \pm 1$ ; we will see below that this is a large- $N$  artifact.

What about the interval where the monomer coupling is  $|x| > x_c$ ? We know that the solution to the mean-field equations is  $\phi = 0$ . Hence, we look at the fluctuations (4.14) around this mean field,

$$S_B^{(2)}[\tilde{\phi}, \tilde{\phi}^*] = \sum_p |\tilde{\phi}_p|^2 + \frac{1}{2x^2} \text{tr}(B(\tilde{\phi})B(\tilde{\phi}^*)) = \sum_p \left(1 - \frac{1}{x^2}\right) |\tilde{\phi}_p|^2, \quad (4.26)$$

where the  $B$  matrix is the block matrix (4.7), and, in the last equality, we took the trace in Fourier space. The free energy is thus

$$f_{1D} = -N \ln(x) + \ln\left(1 - \frac{1}{x^2}\right), \quad |x| > 1, \quad (4.27)$$

which shows the same singularity at the boundary  $x = \pm 1$  as in (4.25).

In the case of the 1d periodic chain, an exact solution of model B is available by transfer matrix methods (see Appendix B). Figure 11 summarizes the mean-field results (4.25) and (4.27) for model B, 1D periodic chain. The free energy density is presented for different numbers of colors, and compared with the exact transfer matrix solution and the homogenous ansatz. We see that the free energy presents a mean-field transition at  $x = 1$  which the solution by transfer matrix does not possess. We believe the transition is not there in the exact solution due to the low dimensionality of the example.

Other examples are more complicated. Again, the mean-field equations lead to a gap equation. There is certainly a homogenous solution, but it is not the only one and generally not the dominant saddle point. Textured mean fields will be energetically superior. Still, what the right mean field to expand around for a general lattice in the interval  $|x| < x_c$  we still don't know.

However, for  $|x| > x_c$ , we can actually find an analytical expression for the effective free energy density by expanding around  $(\phi_0)_{ij} = 0$ . Let's discuss the case of a Bravais lattice with coordination number  $z$ . The fluctuations (4.14) are

$$S_B^{(2)}[\tilde{\phi}, \tilde{\phi}^*] = \sum_{\vec{p}, \hat{e}_i} |\tilde{\phi}_p^{(\hat{e}_i)}|^2 + \frac{1}{2x^2} \text{tr}(B(\tilde{\phi})B(\tilde{\phi}^*)), \quad (4.28)$$

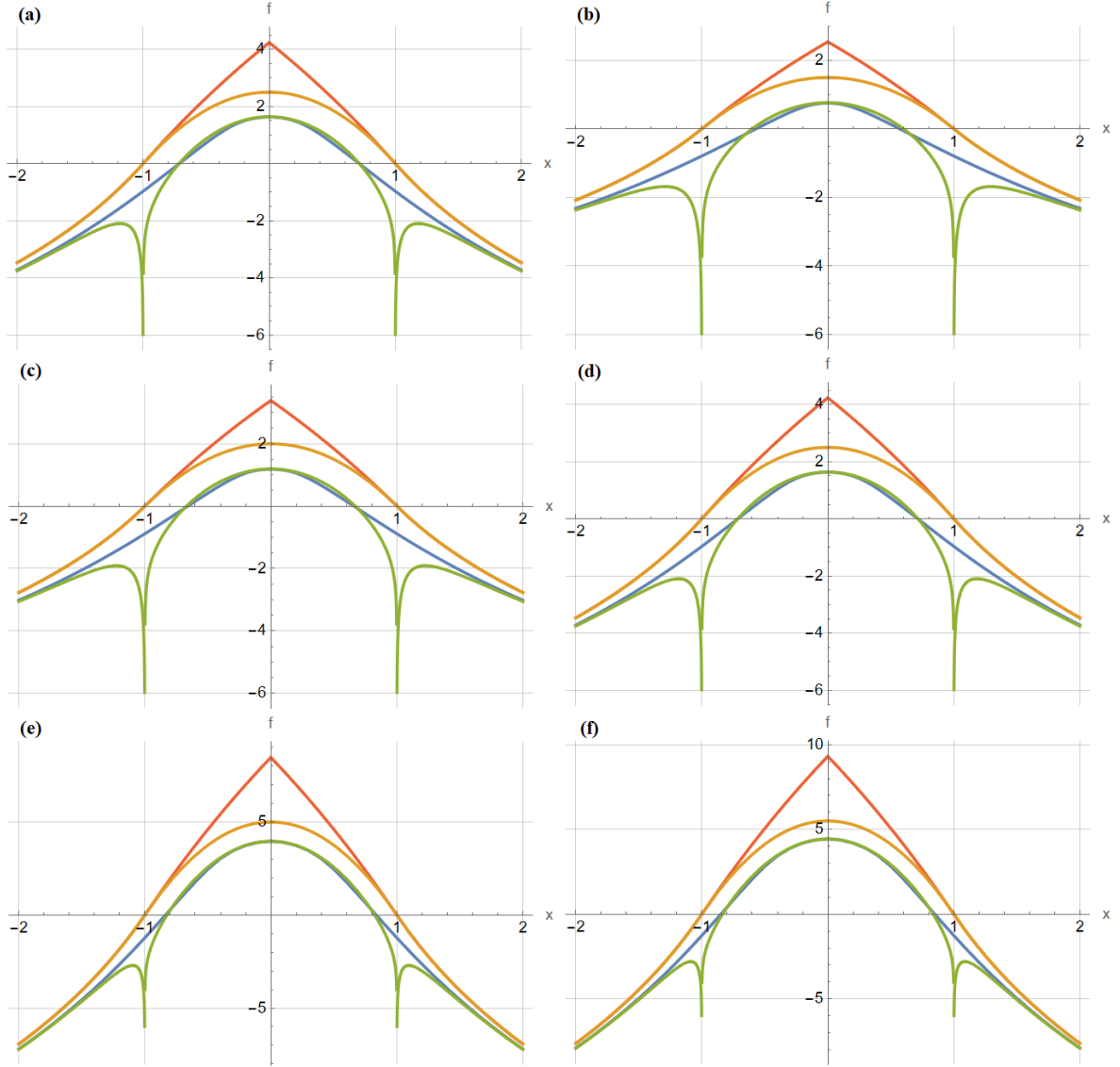


**Figure 4:** 1D, type- $B$  free energy density  $f$  of the exact solution (blue), alternating mean field (orange), and alternating mean field including the one-loop correction (green) as a function of the coupling  $x$ . Moreover, the free energy density of the homogeneous mean field (red) is also plotted. Evens (a)  $N = 2$ , (c)  $N = 4$ , (e)  $N = 10$ , and odds (b)  $N = 3$ , (d)  $N = 5$ , (f)  $N = 11$ . The exact solution (blue) does not present the mean-field transition at  $x = 1$ .

where now we have  $\frac{z}{2}$  link fields in the independent directions  $\hat{e}_i$ . Expanding the

trace term, we get

$$S_B^{(2)} = \sum_{\vec{p}, \hat{e}_i} |\tilde{\phi}_p^{(\hat{e}_i)}|^2 + \frac{1}{2x^2 n_s} \sum_{\vec{p}, \vec{k}, \hat{e}_i, \hat{e}_j} \tilde{\phi}_p^{(\hat{e}_i)} \tilde{\phi}_p^{*(\hat{e}_j)} (e^{-i(\vec{p}+\vec{k})\cdot\hat{e}_i} e^{i\vec{k}\cdot\hat{e}_i}) (e^{-i\vec{k}\cdot\hat{e}_j} e^{i(\vec{p}+\vec{k})\cdot\hat{e}_j}) \quad (4.29)$$

$$= \sum_{\vec{p}, \hat{e}_i} |\tilde{\phi}_p^{(\hat{e}_i)}|^2 + \frac{1}{2x^2 n_s} \sum_{\vec{p}, \hat{e}_i} (-2n_s) |\tilde{\phi}_p^{(\hat{e}_i)}|^2 = \sum_{\vec{p}, \hat{e}_i} \left(1 - \frac{1}{x^2}\right) |\tilde{\phi}_p^{(\hat{e}_i)}|^2, \quad (4.30)$$

where in getting to the last line, we have summed over the Fourier modes  $\vec{k}$  and used the fact that the only contributing factors will be when  $\hat{e}_i = \hat{e}_j$ .

Integrating the Gaussian fluctuations in (4.30), we find that the free energy density is

$$f_B = -N \ln(x) + \frac{z}{2} \ln \left(1 - \frac{1}{x^2}\right), \quad |x| > 1, \quad (4.31)$$

where we see that the saddle point  $(\phi_0)_{ij} = 0$  is stable in the  $|x| > 1$  interval. There is a singularity at the same value of the monomer fugacity  $x_c = \pm 1$ .

The large- $N$  analysis therefore shows a singularity at  $x = 1$  on any Bravais lattice. For the periodic chain, the exact transfer matrix solution shows that there is no such singularity. It could be that this is a special consequence of the enhanced infrared fluctuations in  $D = 1$ . We do not have an exact solution in any  $D > 1$ , and it is possible that the singularity at  $x = 1$  is physical for  $D > 1$ . Indeed, it is possible that there is a Hohenberg-Coleman-Mermin-Wagner argument related to the  $U(1)^{n_s}$  invariance of model B, under which  $\phi_{ij}$  is charged, which might prevent a sharp transition in  $D = 1$ .

## 4.2 Large- $N$ Feynman diagrams

When  $x$  is large, we can study our integral by a diagrammatic expansion familiar from perturbative quantum field theory, using the Feynman rules written in (3.4) and (3.5). The leading contribution to the partition function, independent of the choice of interactions, is (3.3). This produces a term

$$f_0(x) = -N \log x \quad (4.32)$$

in the free energy density  $f \equiv -\frac{1}{n_s} \log Z$ .

As usual we can associate a diagram with a term arising by expanding the exponentiated interaction term  $e^{A\eta\tilde{\eta}\eta\tilde{\eta}}$ . Disconnected diagrams exponentiate and only connected diagrams contribute to the free energy.

At large  $N$ , the structure of the corrections to (4.32) due to the interaction terms simplify dramatically. To identify the dominant diagrams at large  $N$ , the double-line notation is useful: we wish to find diagrams with the most index loops for a given number of interaction vertices.

**Model A.** For model A the dominant diagrams are bubble chains, familiar from many vector-large- $N$  field theories, such as the  $O(N)$  model and the Gross-Neveu model [16, 17]. Each propagator in the bubble chain is the full propagator, which at leading order in large- $N$  is a sum of cactus diagrams (shown below). Let's first use the bare propagator, and then we will see that incorporating all the 1PI corrections will be easy. Since the propagator is ultralocal, each bubble in the chain is labeled by a single site, and neighboring bubbles must be associated with neighboring sites. So a diagram with  $k + 1$  bubbles involves a walk on the graph with  $k$  steps. On an arbitrary homogeneous graph of coordination number  $z$ , therefore, the diagram with  $k + 1$  bubbles contributes

$$\text{Diagram of a chain of } k+1 \text{ bubbles} = \frac{1}{2} N n_s \left( -\frac{\lambda z}{x^2} \right)^k \quad (4.33)$$

where  $\lambda$  is the 't Hooft coupling (set to 1 above). (In more detail: The vertices give a factor of  $(-\lambda/N)^n$ . The index loops give  $N^{n+1}$ . The  $2n$  propagators give  $x^{-2n}$ . The choice of labels on the edges (the number of  $n$ -step walks on the graph) give  $n_s z^n$ . The symmetry factor is  $1/2$  from a reflection in the center of the graph.) The sum of these is

$$f_{\text{bare}}(x, \lambda) = -\frac{1}{2} N \sum_{k=1} \left( -\frac{\lambda z}{x^2} \right)^k = -\frac{1}{2} N \left( -\frac{\frac{z\lambda}{x^2}}{1 - \frac{z\lambda}{x^2}} \right). \quad (4.34)$$

Now let's correct the propagator. The self-energy  $\Sigma$  and the full propagator  $\Delta$  satisfy the Schwinger-Dyson equations

$$\Delta = \frac{1}{x - \Sigma}, \quad \text{Diagrammatic equation: } \text{double line} = \text{single line} + \text{single line} \circlearrowleft \text{double line} + \text{single line} \circlearrowright \text{double line} + \dots \quad (4.35)$$

$$\Sigma_{ij} = -\delta_{ij} \sum_{\ell} A_{i\ell} \Delta_{\ell\ell} + \mathcal{O}(1/N), \quad \text{Diagrammatic equation: } \text{double line} \circlearrowleft \text{double line} = \text{double line} \circlearrowright \text{double line} + \text{double line} \circlearrowleft \text{double line} \circlearrowright \text{double line} + \dots$$

where we have suppressed color and site indices when possible. The second equation shows that at leading order in  $N$  only the diagonal entries in the self-energy are nonzero:  $\Sigma_{ij} = \delta_{ij}\Sigma_j$ . We note that the vertex appearing in the 1PI self-energy is the bare vertex; putting the full corrected vertex described below would double count diagrams. Therefore the Schwinger-Dyson equations reduce to

$$\Sigma_i = - \sum_{\ell} \frac{A_{i\ell}}{x - \Sigma_{\ell}}. \quad (4.36)$$

We do not know how to solve this equation in general. For a translation-invariant graph (of volume  $V$ ), the Green's function is

$$A_{j\ell}^{-1} = \frac{1}{V} \sum_k e^{ik(j-\ell)} D(k), \quad (4.37)$$

and therefore the SD equation is

$$\frac{1}{V} \sum_k e^{ikj} D(k) \tilde{\Sigma}(k) = - \frac{1}{x - \Sigma_j}. \quad (4.38)$$

Assuming translation invariance of the solution,  $\Sigma_j = \Sigma$ ,  $\tilde{\Sigma}(k) = \delta_{k,0} V \Sigma$ , this gives

$$\Sigma(x - \Sigma) = -z \quad (4.39)$$

where  $z = \frac{1}{D(0)}$  is the coordination number of the graph. This is a quadratic equation for  $\Sigma$  whose solution is

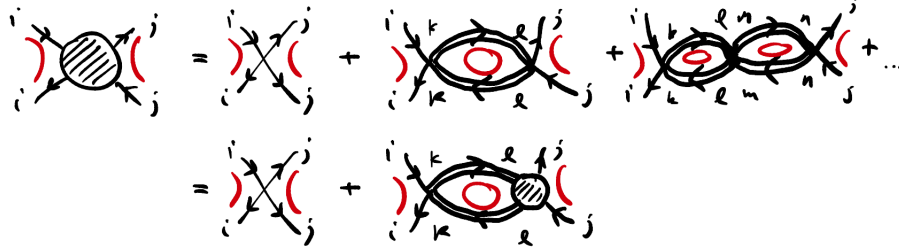
$$\Sigma = \frac{1}{2} \left( x \pm \sqrt{x^2 + 4z} \right) \quad (4.40)$$

Two solutions to the SD equation exist, just as in (4.17). To decide which of the two we shall use, we look at the one that minimizes the action (negative root for  $x > 0$ , and positive root for  $x < 0$ ). Looking back at the form of the full propagator in (4.35), we see that the end result of the propagator corrections from cacti is simply to replace  $x \rightarrow x - \Sigma$ .

The same correction needs to be done to the vertex. At large  $N$ , the full vertex

$\Gamma$  and the bare vertex  $\Gamma_{ij}^0 \equiv \frac{A_{ij}}{2N}$  satisfy the Bethe-Salpeter equation

$$\Gamma_{ij} = \Gamma_{ij}^0 + \sum_{k,l} \Gamma_{ik}^0 \Delta_{kl} \Delta_{kl} \Gamma_{lj} \quad (4.41)$$



where color indices have been suppressed. Assuming that the full vertex is independent of the color indices and using the form of the full propagator  $\Delta$ , we can simplify the equation to

$$\Gamma_{ij} = \frac{A_{ij}}{2N} + \frac{z}{(x - \Sigma)^2} \Gamma_{ij}, \quad (4.42)$$

whose solution is

$$\Gamma_{ij} = \left( \frac{(x - \Sigma)^2}{(x - \Sigma)^2 - z} \right) \frac{A_{ij}}{2N} \equiv \alpha \frac{A_{ij}}{2N}. \quad (4.43)$$

Making the comparison with the bare vertex, we see that the corrections amount to a rescaling by a factor of  $\alpha$ . This change can be taken into account by simply rescaling the 't Hooft coupling  $\lambda \rightarrow \alpha\lambda$ .

All these corrections together make the free energy density to be

$$f_A(x) = f_0(x - \Sigma) + f_{\text{bare}}(x - \Sigma, \alpha\lambda), \quad (4.44)$$

which is the same as Eq. (4.20) that we found using saddle point techniques to leading order in  $1/N$ .

**Model B.** In model B, the dominant diagrams at large  $N$  have a different structure. They are instead rings of bubbles, where each bubble is associated with *the same* pair of neighboring sites. The contribution from the diagram with  $k$  bubbles is

$$= n_{\text{links}} \frac{1}{k} \left( \frac{\lambda}{x^2} \right)^k, \quad (4.45)$$

where  $n_{\text{links}} = n_s z/2$  is the number of links in the graph. The factor of  $1/k$  is a symmetry factor from cyclic permutations of the bubbles. Notice that in this case, the correction is of order  $N^0$ , in contrast with the expression for type A (4.33). In Model B the propagator and vertex corrections are down by powers of  $N$ .

The sum of these diagrams (for a homogeneous graph of valence  $z$ ) is

$$\frac{n_s z}{2} \sum_{k=1} \frac{1}{k} \left( \frac{\lambda}{x^2} \right)^k = \frac{n_s z}{2} \log \left( 1 - \frac{\lambda}{x} \right). \quad (4.46)$$

Therefore

$$\Delta f_B = \frac{z}{2} \log \left( 1 - \frac{\lambda}{x^2} \right), \quad (4.47)$$

which is the same as we found in (4.31). The singularity for type B occurs at  $x = \pm 1$  independent of the graph.

**Model C.** For a graph with no self-loops ( $A_{ii} = 0, \forall i$ ), models B and C are the same at leading order in large  $N$ . The dominant diagrams for model C are:



They only differ by the orientations of the lines.

**Model D.** The large- $N$  diagram story for model D is similar to models B and C, except that the labels on the edges must alternate between successive bubbles, as in:



This means that only rings with an even number of bubbles contribute, giving

$$\Delta f_D = z \log \left( 1 - \left( \frac{\lambda}{x^2} \right)^2 \right). \quad (4.50)$$

## 5 Graph coloring problems

Closely-related ideas may be used to find integral representations for various graph-coloring problems. For example, we can ask how many ways are there to 3-color the links of the honeycomb lattice so that no links sharing a vertex are the same color? This problem was solved exactly by Baxter [18], and has interesting connections to the  $SU(3)_1$  CFT [19, 20] and possible experimental realizations [21]; quantum versions have also been studied [22, 23].

We give two integral representations of this problem. The first and most useful works only for planar lattices. Place  $N_c = 2$  species of grassmann variables  $\eta_i^{\alpha=1,2}$  at each site of a 3-fold coordinated graph. Let  $\tilde{A}_{ij}$  be a signed adjacency matrix of the (planar) graph with the following properties:

- $\tilde{A}_{ij} = -\tilde{A}_{ji}$
- $\prod_{\ell \in \partial p} \tilde{A}_\ell = -1$ , where  $p$  is any elementary plaquette.

This is only possible for planar graphs and is closely related to Kasteleyn's matrix, *i.e.* a choice of  $\mathbb{Z}_2$  gauge field configuration with  $\pi$ -flux through every plaquette. Then the following integral computes the number of 3-colorings of the graph:

$$Z = \int \prod_{\alpha,i} d\eta_i^\alpha \prod_{\langle ij \rangle} (1 + \tilde{A}_{ij} \eta_i^\alpha \eta_j^\alpha) = \int D\eta e^{S[\eta]}. \quad (5.1)$$

(As above, we use the summation convention for the color indices, but not for the lattice site indices.) The idea is again that a nonzero contribution comes only from terms in the expansion of the product where each mode appears once. Each such term involves a choice for each link of either 1 or  $\eta_i^1 \eta_j^1$  or  $\eta_i^2 \eta_j^2$ , which we can regard as the three colors. A choice for a given link is incompatible with the same choice for any link sharing a vertex with it.

We can represent the integrand of Eq. 5.1 in terms of the action

$$S[\eta] = \sum_{\langle ij \rangle} \log(1 + \tilde{A}_{ij} \eta_i^\alpha \eta_j^\alpha). \quad (5.2)$$

The nice thing about  $N_c = 2$  is that  $(\eta_i^\alpha \eta_j^\alpha)^3 = 0$ , which means that the Taylor

expansion of the logarithm terminates at the quartic terms:

$$S[\eta] = \sum_{\langle ij \rangle} \left( \tilde{A}_{ij} \eta_i^\alpha \eta_j^\alpha - \frac{1}{2} A_{ij} \eta_i^\alpha \eta_j^\alpha \eta_i^\beta \eta_j^\beta \right) \quad (5.3)$$

where we used the fact that  $\tilde{A}_{ij} \tilde{A}_{ij} = A_{ij}$  is the unsigned, symmetric adjacency matrix.

Following the ideas discussed previously, we study the action  $S[\eta]$ . That is, decouple the quartic term in (5.3) using an auxiliary link field  $\phi_{ij}$  and do mean-field theory. The HS transformation that trades the quartic interaction is

$$e^{-\frac{1}{2} \sum_{\langle ij \rangle} A_{ij} \eta_i^\alpha \eta_j^\alpha \eta_i^\beta \eta_j^\beta} = \int D\phi e^{\sum_{\langle ij \rangle} -\frac{1}{2} \phi_{ij}^2 + i \tilde{A}_{ij} \phi_{ij} \eta_i^\alpha \eta_j^\alpha}. \quad (5.4)$$

Solving the equation of motion, we get that  $\phi$  at the saddle point is proportional to the number of dimers via  $\phi_{ij}^{\text{saddle}} = i \sum_\alpha \tilde{A}_{ij} \eta_i^\alpha \eta_j^\alpha$ .

After integrating out the  $\eta$  variables, we can rewrite the partition function as a function of the link variables  $\phi$ . That is,  $Z = \int D\phi e^{-S[\phi]}$  where the action  $S[\phi]$  is given by

$$S[\phi] = \sum_{ij} \frac{1}{2} \phi_{ij}^2 - \text{tr} \ln \begin{pmatrix} 0 & \tilde{A}_{ij}(1 + i\phi_{ij}) \\ -\tilde{A}_{ij}(1 + i\phi_{ij}) & 0 \end{pmatrix}. \quad (5.5)$$

We have found a link-field representation which we can study using saddle point techniques. We proceed to do mean-field theory. Assuming the mean field is homogeneous  $\phi_0$ , we find the first variation with respect to this mean field is

$$\left. \frac{\delta S}{\delta \phi_{ij}} \right|_{\phi_0} = \frac{3}{2} n_s \phi_0 - \frac{n_s}{2} \frac{i}{(1 + i\phi_0)} = 0, \quad (5.6)$$

where  $n_s$  is the number of sites, and whose solutions are  $\phi_0^\pm = \pm \frac{\sqrt{3}}{6} + \frac{1}{2}i$ .

We can approximate the number of colorings of the hexagonal lattice by looking at the action at this level  $S_0^\pm \equiv S[\phi_0^\pm]$ ,

$$S_0^\pm = \frac{3}{4} n_s \phi_0^\pm - \frac{n_s \nu_0}{2} \int_{BZ} \frac{d^2 p}{(2\pi)^2} \ln \left( (1 + i\phi_0^\pm) (3 + 2 \cos(\vec{p} \cdot \hat{\delta}_1) - 2 \cos(\vec{p} \cdot \hat{\delta}_2) - 2 \cos(\vec{p} \cdot \hat{\delta}_3)) \right). \quad (5.7)$$

where the  $\hat{\delta}_i$  are the vectors connecting one of the sublattices atoms to their nearest neighbor. Notice that although the locations of the saddle points  $\phi_0^\pm$  do not depend on the lattice, the free energy does.

The partition function will be then given by the sum of the exponential of these two contributions  $Z \approx e^{-n_s S_0^+} + e^{-n_s S_0^-}$ . Its free energy density is

$$f = - \lim_{n_s \rightarrow \infty} \frac{1}{n_s} \ln Z \approx -0.173 , \quad (5.8)$$

which we can compare with Baxter's exact result  $f = -0.190$  [18].

The second integral representation works even for non-planar graphs, though it is more cumbersome. We come back to equation (5.1) but now defined over  $N_c = 3$  species of grassman variables  $\eta_i^{\alpha=1,2,3}$ . A nonzero contribution comes only from products of grassmann at each link  $\langle ij \rangle$  of either  $\eta_i^1 \eta_j^1$ ,  $\eta_i^2 \eta_j^2$  or  $\eta_i^3 \eta_j^3$ . We regard these as our three colors. There's no need to introduce the signed adjacency matrix since all terms in the expansion come with the same overall factor. Thus, we use the unsigned adjacency matrix  $A_{ij}$  for simplicity.

The integral is expressed again in terms of the action (5.3), but doing the appropriate changes mentioned before. Since  $N_c = 3$  now, the difference is that  $(\eta_i^\alpha \eta_j^\alpha)^3 \neq 0$  but  $(\eta_i^\alpha \eta_j^\alpha)^4 = 0$ . Hence, the logarithmic expansion gets up to sextic terms:

$$S[\eta] = \sum_{\langle ij \rangle} A_{ij} \eta_i^\alpha \eta_j^\alpha - \frac{1}{2} A_{ij}^2 \eta_i^\alpha \eta_j^\alpha \eta_i^\beta \eta_j^\beta + \frac{1}{3} A_{ij}^3 \eta_i^\alpha \eta_j^\alpha \eta_i^\beta \eta_j^\beta \eta_i^\gamma \eta_j^\gamma. \quad (5.9)$$

We can decouple both the quartic and sextic interactions by introducing two link fields. The first link field  $\varphi_{ij}$ ,

$$e^{\frac{1}{3}(A_{ij} \eta_i^\alpha \eta_j^\alpha)^3 - \frac{1}{2}(A_{ij} \eta_i^\alpha \eta_j^\alpha)^2} = \int D\varphi e^{\sum_{\langle ij \rangle} -\frac{1}{2} \varphi_{ij}^2 - i A_{ij} \varphi_{ij} \eta_i^\alpha \eta_j^\alpha + \frac{i}{3} A_{ij}^2 \varphi_{ij} \eta_i^\alpha \eta_j^\alpha \eta_i^\beta \eta_j^\beta}, \quad (5.10)$$

trades the interaction terms for a gaussian and quartic term in the  $\eta$  variables, coupled with the field  $\varphi_{ij}$ . This is particularly possible because of the fact that  $(\eta_i^\alpha \eta_j^\alpha)^p = 0$  for  $p \geq 4$ . The second field  $\phi_{ij}$ ,

$$e^{\frac{i}{3} A_{ij}^2 \eta_i^\alpha \eta_j^\alpha \eta_i^\beta \eta_j^\beta \varphi_{ij}} = \int D\phi e^{\sum_{\langle ij \rangle} -\frac{1}{2} \phi_{ij}^2 - \sqrt{\frac{2i\varphi_{ij}}{3}} \phi_{ij} A_{ij} \eta_i^\alpha \eta_j^\alpha} \quad (5.11)$$

decouples the remaining grassmann quartic term.

The partition function one gets, after introducing the two link fields and integrating out the variables  $\eta$ , is  $Z = \int D(\varphi, \phi) e^{-S[\varphi, \phi]}$ , where the action is given

by

$$S[\varphi, \phi] = \sum_{\langle ij \rangle} \left( \frac{1}{2} \phi_{ij}^2 + \frac{1}{2} \varphi_{ij}^2 - \frac{3}{2} \text{tr} \ln \left( A_{ij} - i A_{ij} \varphi_{ij} - A_{ij} \phi_{ij} \sqrt{\frac{2i}{3}} \varphi_{ij} \right) \right). \quad (5.12)$$

Assuming that the mean field is homogeneous in both fields  $\phi_0$  and  $\varphi_0$ , we find that the first variation is

$$\left. \frac{\delta S}{\delta \phi_{ij}} \right|_{\phi_0, \varphi_0} = 2\phi_0 + \frac{\sqrt{\frac{2i\varphi_0}{3}}}{1 - i\varphi_0 - \phi_0 \sqrt{\frac{2i\varphi_0}{3}}} = 0, \quad \left. \frac{\delta S}{\delta \varphi_{ij}} \right|_{\phi_0, \varphi_0} = 2\varphi_0 + \frac{i + \sqrt{\frac{2i}{12\varphi_0}} \phi_0}{1 - i\varphi_0 - \phi_0 \sqrt{\frac{2i\varphi_0}{3}}} = 0. \quad (5.13)$$

There exist four solutions to these equations. The saddle point that minimizes the free energy density gives  $f = -5.037$ , far from the exact value. This result assumes that the dominant saddle is uniform; it may be that an inhomogeneous solution dominates in this case.

## 6 Discussion

The integral representations of dimer problems we have discussed raise a number of interesting questions.

**Monte carlo method.** Under certain symmetry assumptions, the Hubbard-Stratonovich integral in (4.4) has positive measure, and therefore may be efficiently evaluated by sampling<sup>3</sup>. This would be a zero-dimensional analog of auxiliary-field Monte Carlo commonly used to study certain problems of itinerant fermions [24].

For example, consider model B on a bipartite lattice with even  $N$ . Arrange the colors into two groups labelled  $\uparrow a$  and  $\downarrow a$ ,  $a = 1..N/2$ . The operation  $U$  that takes

$$\eta_{A\uparrow a} \rightarrow \tilde{\eta}_{A\downarrow a}, \quad \eta_{B\uparrow a} \rightarrow -\tilde{\eta}_{B\downarrow a}, \quad \eta_{A\downarrow a} \rightarrow -\tilde{\eta}_{A\uparrow a}, \quad \eta_{B\downarrow a} \rightarrow \tilde{\eta}_{B\uparrow a}, \quad \mathbf{i} \rightarrow -\mathbf{i} \quad (6.1)$$

is an antiunitary symmetry of the action of model B after the Hubbard-Stratonovich

---

<sup>3</sup>We are grateful to Tarun Grover for sharing his expertise on this subject.

transformation :

$$\begin{aligned}
S_B &= |\phi_{AB}|^2 + \eta_{A\uparrow a} \eta_{B\uparrow a} \phi_{AB}^* - \tilde{\eta}_{A\uparrow a} \tilde{\eta}_{B\uparrow a} \phi_{AB} + \eta_{A\downarrow a} \eta_{B\downarrow a} \phi_{AB}^* - \tilde{\eta}_{A\downarrow a} \tilde{\eta}_{B\downarrow a} \phi_{AB} \\
&= |\phi|^2 - \psi^T M \psi, \quad \text{with } \psi \equiv \begin{pmatrix} \tilde{\eta}_{A\uparrow a} \\ \tilde{\eta}_{B\downarrow a} \\ \eta_{A\downarrow a} \\ \eta_{B\uparrow a} \end{pmatrix}.
\end{aligned} \tag{6.2}$$

The result of the grassmann integral is  $\int D\psi e^{\psi^T M \psi} = \det M$ . A theorem commonly used in the context of quantum Monte carlo is the following: if  $U^\dagger M U = M$  with  $U$  antiunitary and  $U^2 = -\mathbb{1}$ , then the eigenvalues of  $M$  come in complex-conjugate pairs. Hence  $\det M \geq 0$ . Therefore, at least in this class of examples, the integral over  $\phi$  may be done efficiently by Monte Carlo sampling. We leave its evaluation to future work.

**Related models.** The recent paper [25] considers ensembles of dimer pilings (called ‘multiwebs’) with a different set of weights than we do. Their weights seem to be chosen so that  $Z_N = Z_1^N$ . For their  $n$ -piling problem, they include in their input data a  $\text{SL}(n, \mathbb{R})$  matrix  $\Phi_{ij}^{ab}$  on each link of the graph (called a ‘local  $\text{SL}_n$  system’). Such data can also be incorporated into our models by replacing the quartic term by (*e.g.* generalizing model A)

$$\Phi_{ij}^{ab} \eta_i^a \tilde{\eta}_i^a \eta_j^b \tilde{\eta}_j^b. \tag{6.3}$$

**More general tiling problems.** We can consider tiling a graph by other shapes. For example, consider tiling a region of the square lattice by *wedges* – collections of three neighboring sites that form an ‘L’. An integral representation for the number of such tilings can be obtained by the methods above. Now the input is not just the adjacency matrix of the graph, but a collection of possible tiling objects. We can represent these as a tensor  $A_{ijk}$  with a number of indices equal to the number of sites covered by each object (three, in the case of wedges), which is nonzero if  $ijk$  represents a possible tile, and zero otherwise. In terms of even grassmanns, the partition sum is

$$Z_1(A) = \int D\zeta e^{\frac{1}{3!} \sum_{ijk} A_{ijk} \zeta_i \zeta_j \zeta_k}. \tag{6.4}$$

In terms of ordinary grassmann variables, this can be written as

$$Z_1(A) = \int D(\tilde{\eta}, \eta) e^{\frac{1}{3!} \sum_{ijk} A_{ijk} \eta_i \tilde{\eta}_i \eta_j \tilde{\eta}_j \eta_k \tilde{\eta}_k}. \tag{6.5}$$

A monomer or dimer fugacity can be introduced in the form of quadratic and quartic terms respectively, again preserving the symplectic local gauge invariance.

**Height representations.** In the case of the ordinary dimer model, there is a representation in terms of a periodic height variable. In the case where  $\Gamma$  is a 2d lattice this provides a sort of bosonization of the grassmann integral given above.

For general tilings, the analog of the height variable is more complicated: it takes values in Conway's tiling group [26]. For example, in the case of linear trimers, the analogous variable lives in the 2-torus [8]. In most of the literature on this subject (e.g. [27]), the tiling group is used only to ask whether tilings *exist*, not to count them. How is this bosonic representation related to that in terms of the Hubbard-Stratonovich variable  $\phi$ ?

**Generalized Heilmann-Lieb argument and transitions at finite monomer fugacity.** Heilmann and Lieb demonstrated [6] that in the  $N = 1$  monomer-dimer problem on any lattice, there is no phase transition at finite monomer fugacity  $x \in (0, \infty)$ . Using (2.14) as their main tool, they showed that all zeroes of the partition function lie on the pure-imaginary axis of the complex  $x$  plane. Thus the only real value of  $x$  that can be pinched by the zeros is  $x = 0$ .

All the models we have studied reduce to this problem when  $N \rightarrow 1$ . It is interesting to ask if such an argument exists for the models we have studied for arbitrary  $N$ . For  $N = 2, 3$  and small system size on the periodic chain and square lattice, we have found that the zeroes of the partition function of model *A* are still on the imaginary axis. On the other hand, for model *B* and *C* under the same conditions, the zeroes are in the complex plane. Therefore, the possibility remains open that in models *B* and *C* for  $N > 1$ , these complex roots can pinch the real  $x$  axis at some nonzero value. Indeed, our large- $N$  free energies do have singularities at  $x = 1$ .

We can see how the Heilmann-Lieb argument breaks down for  $N > 1$ , because the Schwinger-Dyson equation is quite different. In order to write the equation, we introduce the notation  $Z(\Gamma, \{N_k\}_k)$  for the dimer piling problem with  $N_k$  colors at site  $k$ . Can it be written as

$$Z(\Gamma, N) \stackrel{?}{=} xZ(\Gamma - i, N - 1) + \sum_j A_{ij}Z(\Gamma - i - j, N - 1)? \quad (6.6)$$

No – because only at the indicated sites are there fewer grassmanns! The simplest

one takes the form

$$Z(\Gamma, \{N_k\}_k) = xZ(\Gamma, \{\dots N_i - 1\}) + \sum_j A_{ij}Z(\Gamma, \{\dots N_i - 1, N_j - 1\}), \quad (6.7)$$

where  $N_k$  is the number of colors at site  $k$ . Thus, for  $N > 1$ , the Schwinger-Dyson equations only close on a much larger collection of inhomogeneous functions.

As is often the case, our models exhibit a tension between tractability and excitement. We showed above that on a bipartite graph, models B and C are the same, and for even  $N$  have an integral representation that can be efficiently evaluated by sampling. However, non-bipartite graphs, where models B and C differ, have the new ingredient of geometrical frustration. We anticipate that many interesting phenomena are hidden there.

**Matrix models.** In the case where we choose the complete graph,  $A_{ij} = 1, \forall i, j$ , these dimer piling models become matrix models like those of [28]. The actions for colorings A, B and C take the form

$$S_A = (\text{tr}(S^\dagger S))^2, \quad S_B = \text{tr}(SS^\dagger SS^\dagger), \quad S_C = \text{tr}(S^T SS^\dagger S^{\dagger T}). \quad (6.8)$$

in terms of the (grassmann-valued) matrix

$$(S)_{\alpha i} \equiv \eta_i^\alpha, (S^\dagger)_{i\alpha} \equiv \tilde{\eta}_i^\alpha. \quad (6.9)$$

These models have an additional symmetry permuting the sites. Such models can have phases that spontaneously break this permutation symmetry (analogous to the translation-symmetry-breaking states found above). For a grassmann-valued matrix, the analog of the eigenvalue distribution (and its topology) is mysterious to us.

**Quantum Dimer Piling Models.** The quantum dimer model associated to a graph  $\Gamma$  is a quantum system whose Hilbert space is spanned by a collection of orthonormal states, each associated to a dimer covering of  $\Gamma$  (e.g. [29, 30]). It can be regarded as a toy model for a system of spin-half particles on  $\Gamma$  in the subspace of states spanned by local singlets. It is a toy model because different local singlet configurations are in fact not orthogonal (for a review, see [31]).

By the same light, we can construct a quantum dimer piling model on  $\Gamma$ . The Hilbert space is spanned by orthonormal states labelled by dimer piling configurations on  $\Gamma$ . This is a toy model for an antiferromagnet with spin- $N/2$  degrees of freedom on the sites of  $\Gamma$  in the same sense as above.

**Consequences for computational complexity?** The dimer model on a generic non-planar graph is a Hard Problem (as described in [15], §13.3). Specifically, computing the permanent of a binary matrix is  $\#P$ -complete. Can we leverage that guaranteed hardness to say something about the difficulty of solving interacting field theories? In this paper we described a formula for the dimer problem on an arbitrary graph in terms of a quartic grassmann integral. Solving this field theory must be at least as hard as the complexity class that contains the non-planar dimer model.

One can also ask about the difficulty of *approximating* the path integral. The difficulty of approximating the permanent is discussed in [15], §13.4. And the conclusion there is that *approximating* the permanent is actually in  $P$ . Does this mean that we should expect a Monte Carlo algorithm for our quartic integral on any graph? It is interesting to compare the algorithm described in [15], §13.5 with the auxiliary-field Monte Carlo algorithm discussed above.

**Acknowledgements.** Thanks to Greg Huber for inspiration about tiling problems. We are grateful to Tarun Grover and Yi-Zhuang You for helpful discussions and comments. This work was supported in part by funds provided by the U.S. Department of Energy (D.O.E.) under cooperative research agreement DE-SC0009919, and by the Simons Collaboration on Ultra-Quantum Matter, which is a grant from the Simons Foundation (652264). JM received travel reimbursement from the Simons Foundation; the terms of this arrangement have been reviewed and approved by the University of California, San Diego in accordance with its conflict of interest policies.

# A Combinatorial problems on dimer pilings

The different colorings, defined in section §3, lead to distinct combinatorial problems when  $N > 1$ . We will be interested in understanding their different interpretations in terms of monomers and dimers fully covering a lattice. Before proceeding, though, we will first need to introduce some notation and definitions.

Let us define a monomer-dimer piling, corresponding to a graph  $\Gamma$ , as a fully-packed configuration of colorless monomers/dimers on  $\Gamma$  such that, at each vertex, the total number of incident monomers and dimers must be  $N$ . We shall also define the monomer piling as the monomer-only packed configuration, and a dimer piling as a dimer-only packed configuration, both satisfying the same constraint as the monomer-dimer piling. For the sake of simplicity, we will interchangeably use piling when referring to the monomer-dimer piling.

Graphically, we will represent such pilings using  $x$ 's on the sites as monomers, and bonds on the links as dimers. As an example, we present below the periodic two-site chain for  $N = 2$  and their corresponding pilings. The graph is presented on the left side of the equality, while the pilings are on the right side. Numbers next to the pilings correspond to the number of equivalent pilings one can get. We identify the first piling as the monomer piling, and the last two as the dimer pilings.



**Figure 5:** Two-site periodic chain and its corresponding monomer-dimer pilings.

Each of these pilings will come with a weight corresponding to its structure, i.e. the monomers at the sites and the dimers at the links of such piling. We weight them with  $1/(N^{n_l} n_l!)$  associated to the number of dimers  $n_l$  at link  $l$ , times  $x^{n_{m_i}}/n_{m_i}!$  associated to the number of monomers  $n_{m_i}$  at site  $i$ . As shall we see, these pilings determine the weights in the combinatorial problem each model defines.

Having defined what a piling is, let us move on to the first coloring, type  $A$ . The combinatorial problem this coloring describes is one where we sum over all monomer-dimer pilings of a given graph  $\Gamma$ . All of these pilings are multiplied by an overall

factor  $N!$  to the total number of sites  $n_s$ . The partition function is thus,

$$Z_N^A(\Gamma, x) = (N!)^{n_s} \sum_{\text{pilings } \mathcal{C} \text{ of } \Gamma} \left( \prod_{\text{sites } i \in \mathcal{C}} \frac{x^{n_{m_i}}}{n_{m_i}!} \right) \left( \prod_{\text{links } l \in \mathcal{C}} \frac{1}{N^{n_l} n_l!} \right). \quad (\text{A.1})$$

The overall factor of model  $A$  can be understood as follows. Recall that dimers of this model comes from the quartic term  $V_A = A_{ij} \eta_i^\alpha \tilde{\eta}_i^\alpha \eta_j^\beta \tilde{\eta}_j^\beta$ . We can think of the type- $A$  dimer as arising from two independent monomer terms: one at site  $i$ , and the other at site  $j$ . Equations (3.8) and (3.11) then say that every site of the graph will be filled with  $N$  pairs of grassman  $\eta_i^\alpha \tilde{\eta}_i^\alpha$  of different colors (either coming from monomers or dimers), the  $N!$  in (3.8) being the number of ways of arranging the  $N$  colors at a single site. Hence, the factor  $(N!)^{n_s}$  in the partition function  $Z_N^A$  is the total number of arrangements at all sites  $n_s$  of the graph  $\Gamma$ .

In contrast, the two remaining models define a much different combinatorial problem. We can no longer understand the dimer as two independent monomers, since model  $B$  and  $C$  interactions couple the color indices of the grassmanns at site  $i$  with those at site  $j$ . Each of the models define a unique way of placing the colorful dimers in the graph  $\Gamma$ . And its weight will correspond to the number of ways of arranging such colorful dimers in the copies  $\mathcal{C}_\eta$  and  $\mathcal{C}_{\tilde{\eta}}$ , as previously mentioned in §3.2, following the rule that at each site of both  $\mathcal{C}_\eta$  and  $\mathcal{C}_{\tilde{\eta}}$  there must be  $N$  different colorful dimers. In the following, we will make sense of this coloring problem and its combinatorial weight by means of a simple example: the last dimer piling in Figure 5.

Let's first consider model  $B$ , whose interaction  $V_B = A_{ij} \eta_i^\alpha \tilde{\eta}_i^\beta \eta_j^\alpha \tilde{\eta}_j^\beta$  decouples colorwise the  $\eta$ 's from the  $\tilde{\eta}$ 's. This type- $B$  dimer paints the link  $\langle ij \rangle$  from  $\mathcal{C}_\eta$  with color  $\alpha$ , and from  $\mathcal{C}_{\tilde{\eta}}$  with color  $\beta$ . That is, each copy of  $\mathcal{C}$  gets to be painted independently, always respecting that, at each site of  $\mathcal{C}_\eta$  and  $\mathcal{C}_{\tilde{\eta}}$ , there must be  $N$  different colorful dimers. So for the simple example, this gives four colorings:

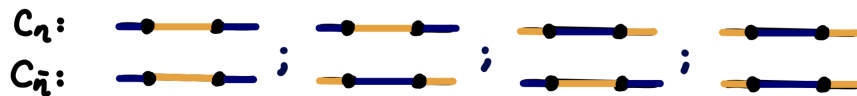


**Figure 6:** All four possibilities of the  $N = 2$  two-site periodic chain using coloring type- $B$ .

On the other hand, model  $C$  paint the copies of such piling in another manner. Instead of fully painting the dimer in  $\mathcal{C}_\eta$  or  $\mathcal{C}_{\tilde{\eta}}$  as in  $B$ , the interaction  $V_C = A_{ij} \eta_i^\alpha \tilde{\eta}_i^\beta \eta_j^\beta \tilde{\eta}_j^\alpha$  paints with the same color half of the dimer in  $\mathcal{C}_\eta$  and the other half in  $\mathcal{C}_{\tilde{\eta}}$ .

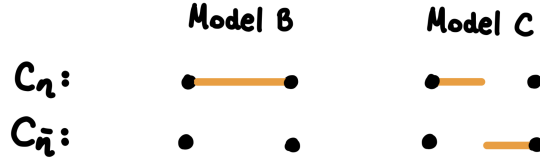


**Figure 7:** Model  $B$  paints the link only in  $\mathcal{C}_\eta$ , while model  $C$  paints half link in  $\mathcal{C}_\eta$  and half in  $\mathcal{C}_{\bar{\eta}}$

One can then paint the example using this type- $C$  coloring rule and find that the number of colorings is again equal to four. One such coloring is presented figure 8. From this example, we can understand why  $B$  and  $C$  are equivalent on bipartite graphs. They both define the coloring counting problem over disjoint sets of sites: model  $B$  over the disjoint sites  $\mathcal{C}_\eta$  and  $\mathcal{C}_{\bar{\eta}}$ , and model  $C$  over the two disjoint sublattices. Furthermore, we can see the action of the transformation in one of the two sublattices of the bipartite graph  $(\eta_i^\alpha, \tilde{\eta}_i^\alpha) \rightarrow (\tilde{\eta}_i^\alpha, -\eta_i^\alpha)$  relating model  $B$  with  $C$ : it maps the disjoint sets from one model to the other.



**Figure 8:** Step-by-step painting of one of the four possible colorings using type- $C$  dimers. Each site of either copy of  $\mathcal{C}$ , satisfies there are  $N = 2$  different colorful dimers.

However, if one considers non-bipartite graphs, the models do differ. There exist piling terms that do not contribute to the partition function of model  $B$ , but do for model  $C$ . As an example, consider the following piling of the three-site chain:

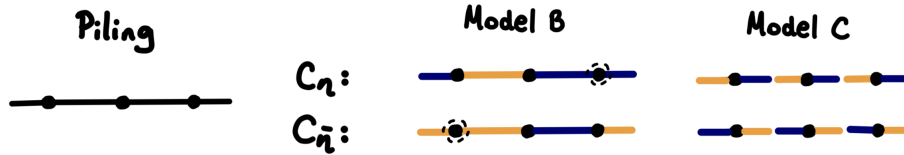


**Figure 9:** Three-site piling, painted using model  $B$  and  $C$ . Using type- $B$  dimers, it's not possible. Circles show where the color rule is violated. Yet, using type- $C$  dimers, two colorings are possible.

Moreover, this piling comes with an overall negative sign while none of the model  $B$  pilings are negative. This begs the question: How can we tell whether a piling

coloring comes with negative sign?

Let us set up the ground by considering what colorings we are sure do come with a positive sign. And let us follow another dimer piling example, in this case of the  $N = 4$  two-site periodic chain and one of its colorings:

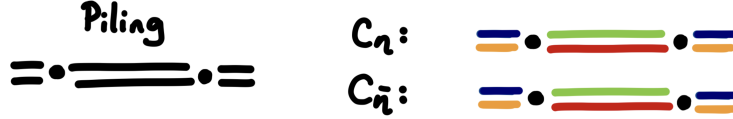


**Figure 10:** Two-site piling for  $N = 4$  and one of its homogeneous colorings, using either type- $B$  or  $C$  dimers. The color structure is the same on  $\mathcal{C}_\eta$  and  $\mathcal{C}_{\tilde{\eta}}$ .

We see that this coloring has the same color structure in both  $\mathcal{C}_\eta$  and  $\mathcal{C}_{\tilde{\eta}}$ . It is an exact copy. We will denote these type of colorings as homogeneous colorings. Since they are the same colorwise, then the contributions associated to this coloring is associated with terms of the form  $\eta_i^a \tilde{\eta}_i^a \eta_j^a \tilde{\eta}_j^a$ , where the superscript  $a$  is any of the colors. The integral of such terms does not produce a minus sign since we just need to move pairs of grassmanns ( $\eta_i^a \tilde{\eta}_i^a$  or  $\eta_j^a \tilde{\eta}_j^a$ ) to integrate them out. Hence, the homogeneous colorings will always come with a positive sign.

What about the signs of colorings where  $\mathcal{C}_\eta$  and  $\mathcal{C}_{\tilde{\eta}}$  are different? Consider another coloring of the mentioned piling using type- $B$  dimers without loss of generality:

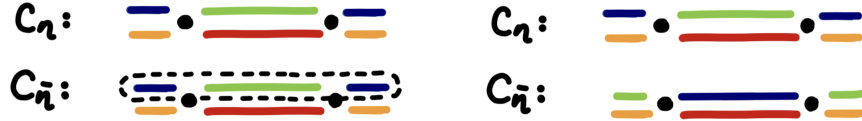


**Figure 11:** On the left, the homogeneous coloring. On the right, a contribution with different colorings in  $\mathcal{C}_\eta/\mathcal{C}_{\tilde{\eta}}$ . We can arrive from the left to the right configuration by moving the circled dimers. This change carries a factor  $(-1)^l$ , where  $l = 2$  is the length of the loop.

As seen in the figure, this coloring can be interpreted as the result of starting from the homogeneous coloring and moving the dimers across the loop shown. Therefore, the sign factor will come from the integral associated to the loop that connects it to any homogeneous coloring. It is not hard to show that this integral carries an overall sign of  $(-1)^l$  where  $l$  is the length of the loop as measured in units of dimers.

With all this in mind, we can see why there are no negative terms in the partition function of model  $B$ : there do not exist odd length loops which alternate colors,

even in non-bipartite graphs. On the contrary, model  $C$  can have these odd length loops and thus, negative terms in its partition function. Even though this raises interesting questions about these models in non-bipartite graphs, we will focus on bipartite lattices and postpone the study on non-bipartite graphs for future work.



**Figure 12:** We can now understand the negative factor coming from this three-site piling. Starting from the homogeneous configuration on the left and moving the dimers along the loop gives a factor of  $(-1)^l$ , where  $l = 3$  is the length of this loop.

Finally, we can add monomers to the mix to get the weight corresponding to these colorings. These will paint both copies of  $\mathcal{C}$  with the same color. The piling weight for model  $B$  is then the number of ways of coloring  $C_\eta$  and  $C_{\tilde{\eta}}$  following the mentioned rules. All together, the partition function is

$$Z_N^B(\Gamma, x) = \sum_{\text{pilings } \mathcal{C} \text{ of } \Gamma} \left( \prod_{\text{sites } i \in \mathcal{C}} \frac{x^{n_{m_i}}}{n_{m_i}!} \right) \left( \prod_{\text{links } l \in \mathcal{C}} \frac{1}{N^{n_l} n_l!} \right) \left( \# \text{ ways coloring } \begin{matrix} C_\eta \\ \text{and } C_{\tilde{\eta}} \end{matrix} \right). \quad (\text{A.2})$$

The description above of the sign of a contribution also applies to monomer-dimer pilings in model B (or in model C on a bipartite graph).

## B Transfer matrix

We can explicitly construct the transfer matrix for the 1D chain for all the models A to C.

**Model A.** The partition function for model A is

$$Z_N^A(\Gamma_0) = \int D(\tilde{\eta}, \eta)^\alpha e^{\sum_i x \eta_i^\alpha \tilde{\eta}_i^\alpha + \frac{1}{N} \sum_i \eta_i^\alpha \tilde{\eta}_i^\alpha \eta_{i+1}^\beta \tilde{\eta}_{i+1}^\beta}, \quad (\text{B.1})$$

where we denote the 1D chain graph as  $\Gamma_0$  with adjacency matrix  $A_{ij} = \delta_{i,j+1} + \delta_{i,j-1}$ .

We can find the structure of the transfer matrix by expanding (B.1) over the sites

$i$  of the chain,

$$Z_N^A(\Gamma_0) = \int D(\tilde{\eta}, \eta)^\alpha \prod_i \left( \sum_{n_{m_i}} \frac{x^{n_{m_i}}}{n_{m_i}!} (\eta_i^\alpha \tilde{\eta}_i^\alpha)^{n_{m_i}} \sum_{n_{d_i}} \frac{1}{N^{n_{d_i}} n_{d_i}!} (\eta_i^\alpha \tilde{\eta}_i^\alpha \eta_{i+1}^\beta \tilde{\eta}_{i+1}^\beta)^{n_{d_i}} \right) \quad (\text{B.2})$$

$$= \int D(\tilde{\eta}, \eta)^\alpha \sum_{\{n_m\}\{n_d\}} \prod_i \left( (\eta_i^\alpha \tilde{\eta}_i^\alpha)^{n_{d_i-1}} \frac{x^{n_{m_i}}}{n_{m_i}!} (\eta_i^\alpha \tilde{\eta}_i^\alpha)^{n_{m_i}} \frac{1}{N^{n_{d_i}} n_{d_i}!} (\eta_i^\alpha \tilde{\eta}_i^\alpha)^{n_{d_i}} \right), \quad (\text{B.3})$$

where, in the last step, we rearrange the terms to get all products of grassmann at site  $i$  more explicit. We proceed by integrating over the grassmanns. Using the identity (3.8), we get

$$Z_N^A(\Gamma_0) = \sum_{\{n_m\}\{n_d\}} \prod_i \left( (N!) \frac{x^{n_{m_i}}}{N^{n_{d_i}} (n_{d_i})! (n_{m_i})!} \delta_{n_{m_i} + n_{d_i} + n_{d_{i-1}}, N} \right) \quad (\text{B.4})$$

$$= \sum_{\{n_d\}} \prod_i \left( (N!) \frac{x^{N - n_{d_i} - n_{d_{i-1}}}}{N^{n_{d_i}} (n_{d_i})! (N - n_{d_i} - n_{d_{i-1}})!} \theta(N - n_{d_i} - n_{d_{i-1}}) \right) \quad (\text{B.5})$$

where  $\theta$  is the Heaviside function which is equal to 1 if  $N - n_{d_i} - n_{d_{i-1}} \geq 0$ , and 0 otherwise. Equation (B.5) defines the transfer matrix connecting link  $\langle i-1, i \rangle$  to  $\langle i, i+1 \rangle$ , summed over the number of dimers on such links.

As a first example, let's look at  $N = 1$ . Here the possible values of the dimers on the links are  $n_d = 0, 1$ . The transfer matrix is hence a  $2 \times 2$  matrix whose rows correspond to the dimer states on the link  $\langle i-1, i \rangle$ , and whose columns correspond to the dimer state on the link  $\langle i, i+1 \rangle$ . That is

$$T_A = \begin{array}{c} \circ \\ \circ \end{array} \begin{array}{c} \circ \quad \text{---} \\ \left( \begin{array}{cc} \times & 1 \\ 1 & 0 \end{array} \right) \end{array} \quad (\text{B.6})$$

and the partition function for a periodic chain is  $Z = \text{tr}(T_A^{n_s})$ . This gives the free energy density  $f = -\lim_{n_s \rightarrow \infty} \frac{1}{n_s} \ln Z$ , the same as the known result  $f = \ln(\frac{1}{2}(x + \sqrt{x^2 + 4}))$ .

For  $N = 2$  the transfer matrix is

$$T_A = \begin{array}{c} \circ \\ \text{---} \\ \text{==} \end{array} 2! \begin{array}{c} \circ \\ \frac{x^2}{2!} \\ x \\ 1 \end{array} \begin{array}{c} \text{---} \\ \frac{x}{2} \\ \frac{1}{2} \\ \circ \end{array} \begin{array}{c} \text{==} \\ \frac{1}{2! 2!} \\ \circ \\ \circ \end{array} \quad (\text{B.7})$$

where the vector space is now generated by no dimers, one dimer and two dimers on the links. Quite generally, for arbitrary  $N$ , the transfer matrix is given by

$$T_{ij}^A = N! \left( \frac{x^{N-i-j}}{(N-i-j)!} \right) \left( \frac{1}{N^j j!} \right) \theta(N-i-j). \quad (\text{B.8})$$

Free energy densities can then be obtained for finite  $N$ . Some examples are plotted in figure 1.

It's difficult to find a general expression for the largest contribution to the partition function for arbitrary  $N$ . However, we can find this for two limits. For  $x \rightarrow \infty$ , the dominating term comes from the configuration with no dimers at any link, fully covered by monomers. Its free energy density is just  $f = -N \ln(x)$ .

For  $x \rightarrow 0$ , the matrix is anti-diagonal and dominated by the homogeneous configuration with  $N/2$  dimers on each link of the chain. In this limit, the free energy density is  $f = -\frac{N}{2} \ln(\frac{2}{e}) - \frac{1}{2} \ln(2)$ . This coincides with the result (4.19) we got using saddle point.

**Models B and C.** We can do the same procedure for the remaining models, and find their corresponding transfer matrix. It's important to point out that the transfer matrix for models  $B$  and  $C$  is now defined over the links of the two copies  $\mathcal{C}_\eta$  and  $\mathcal{C}_{\bar{\eta}}$  (as explained in the appendix A). The rows are the state on the link before  $\langle i-1, i \rangle$  and the columns are the state on the link after  $\langle i, i+1 \rangle$ . The entries of the matrix follow that for each  $n_d$  dimer on the next link, we get a factor of  $n_d! / N^{n_d}$ ; and for  $n_m$  monomers, we get  $x^{n_m} / n_m!$ . Further more there is the constraint that all monomers and dimers must be ( $N$ ) different colors at each site.

To be more clear, let's do the simplest non-trivial example  $N = 2$  for model  $B$ .

The transfer matrix is

$$T_B = \begin{array}{c} \text{0} \\ \text{|||} \end{array} \begin{pmatrix} \text{0} & \text{|||} & \text{|||} & \text{|||} & \text{|||} & \text{|||} & \text{|||} \\ \text{x}^2 & \text{|||} & \text{|||} & \text{|||} & \text{|||} & \text{|||} & \text{|||} \\ \text{x} & \text{0} & \text{|||} & \text{0} & \text{0} & \text{|||} & \text{0} \\ \text{0} & \text{0} & \text{0} & \text{|||} & \text{0} & \text{0} & \text{0} \\ \text{0} & \text{0} & \text{0} & \text{0} & \text{|||} & \text{0} & \text{0} \\ \text{x} & \text{0} & \text{0} & \text{0} & \text{0} & \text{|||} & \text{0} \\ \text{1} & \text{0} & \text{0} & \text{0} & \text{0} & \text{0} & \text{|||} \\ \text{0} & \text{0} & \text{0} & \text{0} & \text{0} & \text{0} & \text{0} \end{pmatrix} \begin{array}{c} \text{|||} \\ \text{|||} \end{array} \quad (\text{B.9})$$

where we have chosen the two colors to be blue and orange. As indicated in (B.9), the basis vectors are labelled as follows: no dimers, one orange dimer in both  $\mathcal{C}_\eta$  and  $\mathcal{C}_{\bar{\eta}}$ , one orange in  $\mathcal{C}_\eta$  and one blue in  $\mathcal{C}_{\bar{\eta}}$ , one blue in both  $\mathcal{C}_\eta$  and  $\mathcal{C}_{\bar{\eta}}$ , and two colorful dimers blue and orange in both  $\mathcal{C}_\eta$  and  $\mathcal{C}_{\bar{\eta}}$ . This transfer matrix is then used to plot figure 4 (a). It is not difficult to construct the matrices for the other  $N$ .

We can again look at the dominant term in the transfer matrix in the two regimes mentioned for model  $A$ . For  $x \rightarrow \infty$ , the sum is dominated by fully covering the chain with monomers, with free energy density  $-N \log x$ . But for  $x \rightarrow 0$ , now we find that the dominant term is the chain with alternating structure:  $N$  dimers on one link and 0 on the next one. We find that the free energy density is given by  $f = \frac{1}{2}N - \frac{1}{4} \ln(2\pi N)$ . This agrees with the alternating mean field we used in the saddle point analysis for model  $B$  up to order  $\ln(N)$ .

Lastly, we can do  $N = 2$  for model  $C$ . The transfer matrix is

$$T_C = \begin{array}{c} \text{0} \\ \text{|||} \end{array} \begin{pmatrix} \text{0} & \text{|||} & \text{|||} & \text{|||} & \text{|||} & \text{|||} & \text{|||} \\ \text{x}^2 & \text{|||} & \text{|||} & \text{|||} & \text{|||} & \text{|||} & \text{|||} \\ \text{x} & \text{0} & \text{|||} & \text{0} & \text{0} & \text{|||} & \text{0} \\ \text{0} & \text{0} & \text{0} & \text{|||} & \text{0} & \text{0} & \text{0} \\ \text{0} & \text{0} & \text{0} & \text{0} & \text{|||} & \text{0} & \text{0} \\ \text{x} & \text{0} & \text{0} & \text{0} & \text{0} & \text{|||} & \text{0} \\ \text{1} & \text{0} & \text{0} & \text{0} & \text{0} & \text{0} & \text{|||} \\ \text{0} & \text{0} & \text{0} & \text{0} & \text{0} & \text{0} & \text{0} \end{pmatrix} \begin{array}{c} \text{|||} \\ \text{|||} \end{array} \quad (\text{B.10})$$

where the difference now is that the basis vectors are labelled with half of the dimer

painted with one color and the other half with another, and the entries are diagonal within that subspace.

This transfer matrix also shows the negative terms that were discussed in appendix A. We can see this by taking the partition function  $Z = \text{tr}(T^{n_s})$  of any odd number of sites. For example, for  $n_s = 1$ , the partition function is  $Z = x^2 - 1$ . These terms come from the fully covered configuration by monomers ( $x^2$ ), and the dimers-only configuration ( $-1$ ) respectively.

## C Details of saddle point calculation

**Uniform saddle point for each link direction in model A.** We have studied model A using the homogeneous solution, independent of the link direction. This was possible since there was no preferred direction, as the action (4.3) only depends on the symmetric  $A_{ij}$  matrix. We can ask how this picture would change if we instead consider a weighted matrix that depends on the direction of the lattice vectors.

Let's consider the action of model A (4.3) on a Bravais lattice with weight  $\omega_i$  in the direction  $\hat{e}_i$ :

$$S_A[\phi, \phi^*] = \sum_{\vec{r}, i} |\phi_{\vec{r}, \vec{r} + \hat{e}_i}^{(\hat{e}_i)}|^2 - \sum_{\vec{r}} \ln |x + \sum_i \omega_i (\phi_{\vec{r}, \vec{r} + \hat{e}_i}^{(\hat{e}_i)} + \phi_{\vec{r} - \hat{e}_i, \vec{r}}^{(\hat{e}_i)*})|. \quad (\text{C.1})$$

Taking the first variation of the action,

$$\frac{\delta S}{\delta \phi_{\vec{r}, \vec{r} + \hat{e}_i}^{(\hat{e}_i)*}} = \phi_{\vec{r}, \vec{r} + \hat{e}_i}^{(\hat{e}_i)} - \frac{\omega_i}{x + \sum_j \omega_j (\phi_{\vec{r} + \hat{e}_i, \vec{r} + \hat{e}_i + \hat{e}_j}^{(\hat{e}_j)} + \phi_{\vec{r} + \hat{e}_i - \hat{e}_j, \vec{r} + \hat{e}_i}^{(\hat{e}_j)*})} \quad (\text{C.2})$$

$$\frac{\delta S}{\delta \phi_{\vec{r}, \vec{r} + \hat{e}_i}^{(\hat{e}_i)}} = \phi_{\vec{r}, \vec{r} + \hat{e}_i}^{(\hat{e}_i)*} - \frac{\omega_i}{x + \sum_j \omega_j (\phi_{\vec{r}, \vec{r} + \hat{e}_j}^{(\hat{e}_j)} + \phi_{\vec{r} - \hat{e}_j, \vec{r}}^{(\hat{e}_j)*})}. \quad (\text{C.3})$$

We see that the mean field is still real ( $\phi_0^{(\hat{e}_i)} = \phi_0^{(\hat{e}_i)*}$ ) with solution given by

$$\phi_0^{(\hat{e}_i)} = \omega_i \left( \frac{-x \pm \sqrt{x^2 + 8\omega^2}}{4\omega^2} \right), \quad (\text{C.4})$$

where  $\omega^2 = \sum_i \omega_i^2$ . This reduces to the case with homogeneous mean field in all directions (4.17) when  $\omega_i = 1$  as expected.

We can take the second variation with respect to the field  $\phi$  to find the second-order fluctuations (4.14) around the mean field  $\phi_0^{(\hat{e}_i)}$ ,

$$S_A^{(2)}[\tilde{\phi}, \tilde{\phi}^*] = \sum_{\vec{r}, i} |\tilde{\phi}_{\vec{r}, \vec{r} + \hat{e}_i}^{(\hat{e}_i)}|^2 + \sum_{\vec{r}, i, j} \phi_0^{(\hat{e}_i)} \phi_0^{(\hat{e}_j)} \left( \tilde{\phi}_{\vec{r}, \vec{r} + \hat{e}_i}^{(\hat{e}_i)} \tilde{\phi}_{\vec{r} - \hat{e}_j, \vec{r}}^{(\hat{e}_j)*} + \frac{1}{2} \tilde{\phi}_{\vec{r}, \vec{r} + \hat{e}_i}^{(\hat{e}_i)} \tilde{\phi}_{\vec{r}, \vec{r} + \hat{e}_j}^{(\hat{e}_j)} + \frac{1}{2} \tilde{\phi}_{\vec{r}, \vec{r} + \hat{e}_i}^{(\hat{e}_i)*} \tilde{\phi}_{\vec{r} + \hat{e}_i - \hat{e}_j, \vec{r} + \hat{e}_i}^{(\hat{e}_j)*} \right), \quad (\text{C.5})$$

which we can simplify by going to Fourier space

$$S_A^{(2)}[\tilde{\phi}, \tilde{\phi}^*] = \sum_{\vec{p}, \hat{e}_i} |\tilde{\phi}_{\vec{p}}^{(\hat{e}_i)}|^2 + \sum_{\vec{p}, \hat{e}_i, \hat{e}_j} \phi_0^{(\hat{e}_i)} \phi_0^{(\hat{e}_j)} \left( \tilde{\phi}_{\vec{p}}^{(\hat{e}_i)} \tilde{\phi}_{\vec{p}}^{*(\hat{e}_j)} e^{i\vec{p} \cdot \hat{e}_j} + \frac{1}{2} \tilde{\phi}_{\vec{p}}^{(\hat{e}_i)} \tilde{\phi}_{-\vec{p}}^{(\hat{e}_j)} + \frac{1}{2} \tilde{\phi}_{\vec{p}}^{*(\hat{e}_i)} \tilde{\phi}_{-\vec{p}}^{*(\hat{e}_j)} e^{i\vec{p} \cdot (\hat{e}_i - \hat{e}_j)} \right). \quad (\text{C.6})$$

We can find the spectrum of the Gaussian fluctuations to get the effective free energy density. We get

$$f_A = N \left( \sum_i |\phi_0^{(\hat{e}_i)}|^2 - \ln \left| x + \sum_i 2\omega_i \phi_0^{(\hat{e}_i)} \right| \right) + \frac{\nu_0}{2} \int_{BZ} \frac{d^d p}{(2\pi)^d} \ln \left( 1 + \sum_i 2|\phi_0^{(\hat{e}_i)}|^2 \cos(\vec{p} \cdot \hat{e}_i) \right), \quad (\text{C.7})$$

where  $\nu_0$  is the unit cell volume,  $z$  is the coordination number, and  $\hat{e}_i$  are the primitive vectors. Again, this simplifies to (4.20) when taking the limit  $\omega_i = 1$ .

Singularities arise from the  $1/N$  corrections at  $x = 0$  where the argument of the log function becomes zero. For example, for the triangular lattice, this can only happen when one of the weights  $\omega_1 = 0$  along one of the directions. In this limit, the triangular lattice model degenerates into the square lattice dimer model. This is in accordance with the fact that the square-lattice dimer model is indeed critical when  $N \rightarrow 1$ , with algebraic decay of correlators [4, 5, 7].

**Uniform saddle point in model B.** As we saw in figure 3, the homogeneous solution is not the energetically superior mean field. Yet, there could be instances where the true mean field is given by  $(\phi_0)_{ij} = \phi_0$ , like certain particular observables. This motivates the detailed analysis of the homogeneous ansatz, which we will present here.

Using the homogeneous ansatz  $\phi_0$  in the  $1D$  periodic chain considered, we find that the action is

$$S_B[\phi, \phi^*] = n_s |\phi_0|^2 - \frac{1}{2} \text{tr} \ln \begin{pmatrix} -B(\phi_0^*) & -x\mathbb{1} \\ x\mathbb{1} & B(\phi_0) \end{pmatrix}, \quad (\text{C.8})$$

where the block matrix  $B$  is in momentum space

$$B(\phi_0) = -2i\phi_0 \sum_p \sin(p) |p\rangle\langle p| . \quad (\text{C.9})$$

We can simplify the action to get

$$S_B[\phi_0, \phi_0^*] = n_s |\phi_0|^2 - \frac{1}{2} \sum_p \ln(x^2 + 4|\phi_0|^2 \sin^2(p)), \quad (\text{C.10})$$

and minimize the action with respect to  $\phi_0$

$$\frac{\delta S_B}{\delta \phi_0^*} = n_s \phi_0 - \frac{1}{2} \sum_p \frac{4\phi_0 \sin^2(p)}{x^2 + 4|\phi_0|^2 \sin^2(p)} = 0. \quad (\text{C.11})$$

The solution to this gap equation is presented in figure 3.

We can do the same procedure to find the gap equation for different lattices. If we consider Bravais lattices, we find that the gap equation is

$$\phi_0 = \frac{\nu_0}{z} \int \frac{d^d p}{(2\pi)^d} \left( \frac{4\phi_0 (\sum_{\hat{e}_i} \sin(\vec{p} \cdot \hat{e}_i))^2}{x^2 + 4|\phi_0|^2 (\sum_{\hat{e}_i} \sin(\vec{p} \cdot \hat{e}_i))^2} \right), \quad (\text{C.12})$$

where  $\nu_0$  is the unit cell volume,  $z$  is the coordination number, and  $\hat{e}_i$  are the primitive vectors.

Figure 13 shows the solution of (C.12) for the  $d$ -dimensional cube. The different curves represent  $\phi_0$  as a function of the monomer fugacity  $x$ , for  $d = 1, 2, 3$ . For all  $d$ , two special points can be spotted in the plot  $x = 0$  and  $x = \pm 1$ .

We proceed to calculate the behavior around those points. Let's first start with the points  $x_c = \pm 1$  where the gap becomes zero. Expanding (C.12) about  $x = x_c - \delta x$  and  $\phi = \delta \phi$ , we get

$$|\delta \phi| = \frac{1}{\sqrt{\alpha x_c}} (\delta x)^{\frac{1}{2}}, \quad (\text{C.13})$$

where the value of the constant  $\alpha$  is given by

$$\alpha = \frac{2\nu_0}{z x_c^4} \int \frac{d^d p}{(2\pi)^d} \left( \sum_{\hat{e}_i} \sin(\vec{p} \cdot \hat{e}_i) \right)^4. \quad (\text{C.14})$$

We see that the scaling near  $x_c$  is of the square-root form  $\delta \phi \sim (x_c - x)^{\frac{1}{2}}$ , independent of the lattice details.

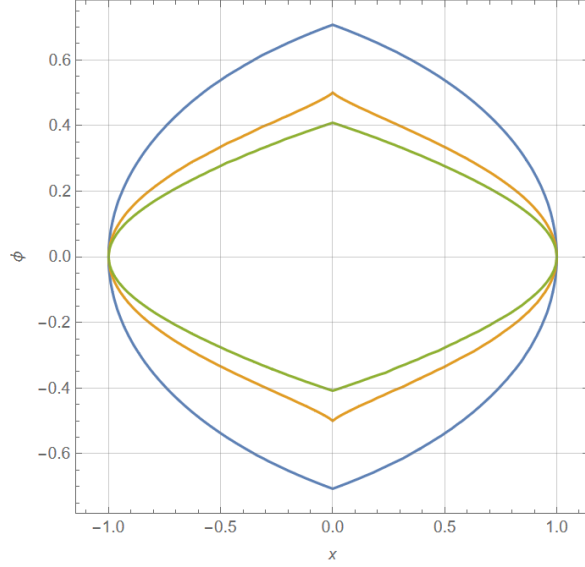


**Figure 13:** Order parameter  $\phi$  as a function of  $x$  for different dimensions  $d = 1, 2, 3$  where the blue curve is  $d = 1$ , the orange curve is  $d = 2$  and the green curve is  $d = 3$ . Two critical points can be seen at  $x = 0, x = \pm 1$ .

Next, let's consider the behavior of the gap  $\phi_c$  at  $x = 0$ . Once again, we can find the scaling by expanding (C.12) around  $\phi = \phi_c + \delta\phi$  and  $x = \delta x$  to find

$$\delta\phi = -\delta x^2 \left( \frac{\nu_0}{2z\phi_c} \int \frac{d^d p}{(2\pi)^d} \frac{1}{\delta x^2 + 4\phi_c^2 (\sum_{\hat{e}_i} \sin(\vec{p} \cdot \hat{e}_i))^2} \right). \quad (\text{C.15})$$

We see that there will be factors of  $\delta x$  coming from the integral. Low energy degrees of freedom will play an important role in evaluating the scaling around  $x = 0$ . Assuming that there's a Fermi surface, then the scaling is  $\delta\phi \sim |\delta x|$ . In contrast, if we have Dirac points, then it will depend on the number of dimensions. For example, for the honeycomb lattice, the scaling near the gap is  $\delta\phi \sim \delta x^2 \ln \delta x$ .

**Gauge fixing for model B.** We have seen that the spectrum of (4.22) has zero eigenvalues, making the matrix singular. We have argued that this is a result of the gauge redundancy  $U : \phi_{ij} \rightarrow e^{i(\theta_i + \theta_j)} \phi_{ij}$  of the model. We will show how to lift the redundancy using the procedure known as gauge fixing, introduced by Faddeev and Popov [32].

Let us denote the gauge condition that we will impose by  $g(\phi, \phi^*) = 0$ , where we

take

$$g(\phi, \phi^*) = \phi_{i,i+1} - \phi_{i,i+1}^*, \quad (\text{C.16})$$

and consider the expression defined by the group integral

$$\Delta_g^{-1}[\phi, \phi^*] = \int DU \delta(g(\phi^U, \phi^{*U})), \quad (\text{C.17})$$

where  $\phi^U, \phi^{*U}$  are configurations related by the gauge transformation  $U$  to  $\phi, \phi^*$  respectively.

The quantity  $\Delta_g[\phi, \phi^*]$  is known as the Faddeev-Popov determinant. This quantity is gauge invariant by construction. This can be shown to be

$$\Delta_g[\phi, \phi^*] = \det \left| \frac{\delta g}{\delta \theta} \right|_{g=0} = \prod_{i=1}^{n_s} |2\phi_{i,i+1}|. \quad (\text{C.18})$$

Since the mean field we are expanding around is

$$(\phi_0)_{i,i+1} = \phi_\pi (1 + e^{i\pi x_i}), \quad (\text{C.19})$$

we just need to impose the gauge-fixing condition on the links  $\langle 2i, 2i+1 \rangle$ . Else, the gauge would be singular.

Let's insert the identity (C.17) in the path integral for the 1D periodic chain we have been discussing,

$$Z_B^N = \int D(\phi, \phi^*) \int DU \delta(g(\phi, \phi^*)) \Delta_g[\phi, \phi^*] e^{-NS_B[\phi, \phi^*]} \quad (\text{C.20})$$

$$= (2\pi)^{\frac{n_s}{2}} \int D(\phi, \phi^*) \delta(g(\phi, \phi^*)) \Delta_g[\phi, \phi^*] e^{-NS_B[\phi, \phi^*]}, \quad (\text{C.21})$$

where, in the last line, we changed the order of integration and get a factor of the volume of the gauge group  $(2\pi)^{n_s/2}$ . The result after gauge fixing (C.21) is a mixture of real and complex fields: real fields on the links  $\langle 2i, 2i+1 \rangle$  and complex fields on the links  $\langle 2i-1, 2i \rangle$ . We will denote the real fields as  $\varphi$  and the complex still as  $\phi$ .

We can proceed with the saddle point analysis. Expanding around the alternating mean field  $(\phi_0)_{2i-1,2i} = 2\phi_\pi$  and  $\varphi_{2i,2i+1} = 0$ , we get that the action governing the second-order fluctuations (4.14) is

$$S^{(2)}[\varphi, \phi, \phi^*] = \sum_i (1-x^2) |\tilde{\phi}_{2i-1,2i}|^2 + \sum_i 2(1-x^2) (\tilde{\varphi}_{2i,2i+1})^2, \quad (\text{C.22})$$

leading to the effective partition function (4.15) to be

$$\begin{aligned} Z_B^N(\Gamma_0) &= (8\pi\phi_\pi)^{\frac{n_s}{2}} e^{-NS_0} \int D(\phi, \phi^*) e^{-N(1-x^2)\sum_i |\tilde{\phi}_{2i-1,2i}|^2} \int D\varphi e^{-2N(1-x^2)\sum_i \tilde{\varphi}_{2i,2i+1}^2} \\ &= (8\pi\phi_\pi)^{\frac{n_s}{2}} e^{-NS_0} \left( (1-x^2)^{-\frac{n_s}{2}} \right) \left( \left( \frac{N}{\pi} \right)^{\frac{n_s}{4}} (2(1-x^2))^{-\frac{n_s}{4}} \right), \end{aligned} \quad (\text{C.23})$$

where  $\phi_\pi^2 = \frac{1}{4}(1-x^2)$ . We see that we get terms proportional to  $N^{\frac{n_s}{4}}$  due to the measure of the integral  $D\varphi = \prod_i \left( \frac{N}{\pi} d\tilde{\varphi}_{2i,2i+1} \right)$ .

We finally find that the free energy density is

$$f_{1D} = \frac{N}{2}(1-x^2) - \frac{1}{4} \ln(8\pi N) + \frac{1}{2} \ln(1-x^2), \quad |x| < 1. \quad (\text{C.24})$$

## References

- [1] P. W. Kasteleyn, “The statistics of dimers on a lattice: I. The number of dimer arrangements on a quadratic lattice,” *Physica* **27** (1961), no. 12 1209–1225. [3](#), [5](#)
- [2] H. N. Temperley and M. E. Fisher, “Dimer problem in statistical mechanics-an exact result,” *Philosophical Magazine* **6** (1961), no. 68 1061–1063. [3](#)
- [3] M. E. Fisher, “Statistical mechanics of dimers on a plane lattice,” *Physical Review* **124** (1961), no. 6 1664. [3](#)
- [4] P. W. Kasteleyn, “Dimer statistics and phase transitions,” *Journal of Mathematical Physics* **4** (1963), no. 2 287–293. [3](#), [20](#), [46](#)
- [5] M. E. Fisher and J. Stephenson, “Statistical mechanics of dimers on a plane lattice. II. Dimer correlations and monomers,” *Physical Review* **132** (1963), no. 4 1411. [3](#), [20](#), [46](#)
- [6] O. J. Heilmann and E. H. Lieb, “Theory of monomer-dimer systems,” in *Statistical Mechanics*, pp. 45–87. Springer, 1972. [3](#), [6](#), [34](#)

- [7] P. Fendley, R. Moessner, and S. L. Sondhi, “Classical dimers on the triangular lattice,” *Physical Review B* **66** (2002), no. 21 214513. [3](#), [20](#), [46](#)
- [8] A. Ghosh, D. Dhar, and J. L. Jacobsen, “Random trimer tilings,” *Physical Review E* **75** (2007), no. 1 011115. [3](#), [34](#)
- [9] D. Dhar and R. Rajesh, “Entropy of fully packed hard rigid rods on d-dimensional hypercubic lattices,” *Physical Review E* **103** (2021), no. 4 042130. [3](#)
- [10] G. Huber, C. Knecht, W. Trump, and R. M. Ziff, “Riddles of the sphinx tilings,” *arXiv e-prints* (Apr., 2023) arXiv:2304.14388, [2304.14388](#). [3](#)
- [11] S. Samuel, “The use of anticommuting variable integrals in statistical mechanics. I. The computation of partition functions,” *Journal of Mathematical Physics* **21** (1980), no. 12 2806–2814. [3](#)
- [12] S. Samuel, “The use of anticommuting variable integrals in statistical mechanics. II. The computation of correlation functions,” *Journal of Mathematical Physics* **21** (1980), no. 12 2815–2819. [3](#)
- [13] S. Samuel, “The use of anticommuting variable integrals in statistical mechanics. III. Unsolved models,” *Journal of Mathematical Physics* **21** (1980), no. 12 2820–2833. [3](#), [17](#)
- [14] G. t’Hooft, “A planar diagram theory for strong interactions,” *Nuclear Physics. B* **72** (1974), no. 3 461–473. [9](#)
- [15] C. Moore and S. Mertens, *The nature of computation*. OUP Oxford, 2011. [10](#), [36](#)
- [16] S.-K. Ma, “Critical exponents for charged and neutral bose gases above  $\lambda$  points,” *Physical Review Letters* **29** (1972), no. 19 1311. [25](#)
- [17] D. J. Gross and A. Neveu, “Dynamical symmetry breaking in asymptotically free field theories,” *Physical Review D* **10** (1974), no. 10 3235. [25](#)
- [18] R. Baxter, “Colorings of a hexagonal lattice,” *Journal of Mathematical Physics* **11** (1970), no. 3 784–789. [29](#), [31](#)

- [19] J. Kondev and C. L. Henley, “Kac-Moody symmetries of critical ground states,” *Nuclear Physics B* **464** (1996), no. 3 540–575. [29](#)
- [20] J. Kondev, J. de Gier, and B. Nienhuis, “Operator spectrum and exact exponents of the fully packed loop model,” *Journal of Physics A: Mathematical and General* **29** (1996), no. 20 6489. [29](#)
- [21] P. C. Verpoort, J. Simmons, and C. Castelnovo, “Color-dependent interactions in the three coloring model,” *Physical Review B* **98** (2018), no. 2 024403. [29](#)
- [22] C. Castelnovo, C. Chamon, C. Mudry, and P. Pujol, “Quantum three-coloring dimer model and the disruptive effect of quantum glassiness on its line of critical points,” *Physical review B* **72** (2005), no. 10 104405. [29](#)
- [23] C. Castelnovo, C. Chamon, C. Mudry, and P. Pujol, “From quantum mechanics to classical statistical physics: Generalized Rokhsar–Kivelson Hamiltonians and the “stochastic matrix form” decomposition,” *Annals of Physics* **318** (2005), no. 2 316–344. [29](#)
- [24] F. Assaad and H. Evertz, “World-line and determinantal quantum Monte Carlo methods for spins, phonons and electrons,” in *Computational Many-Particle Physics*, pp. 277–356. Springer, 2008. [32](#)
- [25] D. C. Douglas, R. Kenyon, and H. Shi, “Dimers, webs, and local systems,” *Transactions of the American Mathematical Society* (2022) [2205.05139](#). [33](#)
- [26] W. P. Thurston, “Conway’s tiling groups,” *The American Mathematical Monthly* **97** (1990), no. 8 757–773. [34](#)
- [27] C. Kenyon and R. Kenyon, *Tiling a polygon with rectangles*. Ecole Normale Supérieure de Lyon. Laboratoire de l’Informatique du . . . , 1992. [34](#)
- [28] S. A. Hartnoll, E. A. Mazenc, and Z. D. Shi, “Topological order in matrix Ising models,” *SciPost Phys.* **7** (2019), no. 6 081, [1908.07058](#). [35](#)
- [29] D. S. Rokhsar and S. A. Kivelson, “Superconductivity and the Quantum Hard-Core Dimer Gas,” *Phys. Rev. Lett.* **61** (1988) 2376–2379. [35](#)

- [30] R. Moessner and S. L. Sondhi, “Resonating valence bond phase in the triangular lattice quantum dimer model,” *Physical Review Letters* **86** (2001), no. 9 1881. [35](#)
- [31] R. Moessner and K. S. Raman, “Quantum dimer models,” in *Introduction to frustrated magnetism: materials, experiments, theory*, pp. 437–479. Springer, 2010. [35](#)
- [32] L. Faddeev and V. Popov, “Feynman diagrams for the Yang-Mills field,” *Physics Letters B* **25** (1967), no. 1 29–30. [48](#)